Detecting and Quantifying Area Wide Permafrost Change

Christoph Klug [(1)], Erik Bollmann [(1)], Lorenzo Rieg [(1)], Maximilian Sproß [(1)], Rudolf Sailer [(1,2)] & Johann Stötter [(1,2)]

[(1)] Institute of Geography, University of Innsbruck, Austria
[(2)] alpS – Centre for Climate Change Adaption, Innsbruck, Austria

1 Introduction

Permafrost and rock glaciers are widespread phenomena in higher altitudes of the European Alps. Since mountain permafrost is very sensitive to the effects of the ongoing climate change (French 1996; Haeberli & Gruber 2009) and its degradation plays a key role in the possible increase of hazard potentials (Kneisel et al. 2007; Noetzli et al. 2007; Sattler et al. 2011), the monitoring of permafrost areas is of particular interest.

Due to the complexity of detecting ground ice, the knowledge regarding permafrost occurence and its distribution is currently very limited for wide areas in the Alps (Kellerer-Pirklbauer 2005; Sattler et al. 2011). The detection and consequent monitoring of possible permafrost areas based on high resolution data (e. g. airborne laser scanning, ALS, and aerial photogrammetry) has the potential to reveal possible permafrost zones which might require further investigations. For an area-wide monitoring of rock glaciers remote sensing techniques have gained in importance in recent years (Kääb 2008).

This research within the permAfrost project focused on three research sites, situated in Tyrol (Stubai and Ötztal Alps) and Vorarlberg (Montafon Range) and ranging from a local to a regional scale.

For detailed investigations based on ALS, four rock glaciers have been chosen for the quantification of surface changes (cf. Fig. 1). These are (1) Reichenkar (RK), (2) Schrankar (SK), (3) Äusseres Hochebenkar (AHK) and (4) Ölgrube rock glacier (OGR). Especially the AHK has a long record of scientific research of nearly 75 years. Different approaches such as terrestrial methods (e. g. geomorphological mapping, geodetic surveys and geological observations), remote sensing (e. g. photogrammetry) and automatic monitoring of different parameters (e. g. ground temperature, climate) have been applied to study the complex rock glacier. Using ALS data in rock glacier research, especially for validating the photogrammetric derived digital elevation models (DEMs), and for calculating flow velocities is an innovative method for area-wide investigations on permafrost.

In a second step, the workflow established on the above mentioned rock glaciers has been adapted to the whole area of Montafon (Vorarlberg). The calculation of surface changes, which has been done on these single rock glaciers, was applied for

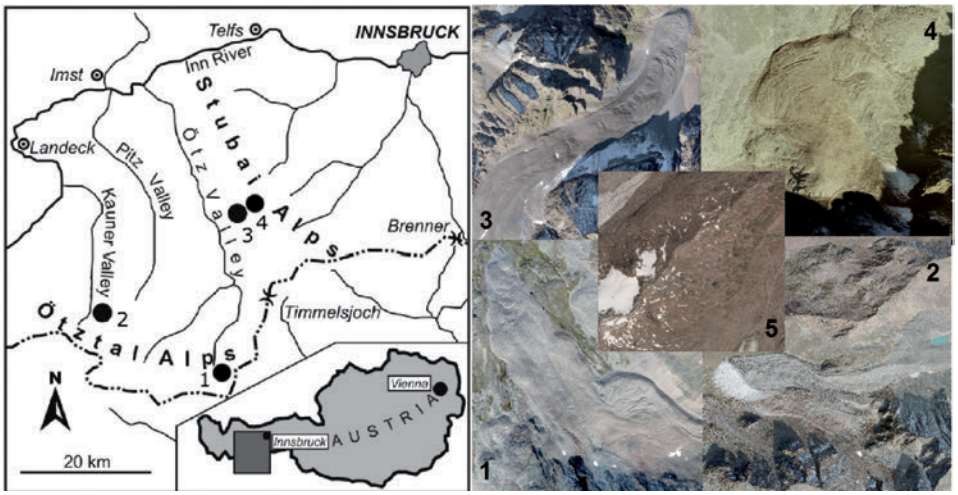

Figure 1: Location of the study sites: Hochebenkar (1), Innere Ölgrube (2), Reichenkar (3), Schrankar (4) and Rofenberg (5). Right side: Orthophotographs from AHK (1), OGR (2) RK (3), SK (4) and Rofenberg with tongue of Hintereisferner (5)

the whole region to detect area wide surface changes. The presented study shows an objective and reproducible approach to assess rock glacier activities (relict or intact) based on two parameters, namely the magnitude and standard deviation of rock glacier thickness changes, calculated from ALS data.

Furthermore, a study site has been installed at Rofenberg for comparing and validating the remote sensing derived insights about permafrost induced surface changes with direct field measurements (e. g. bottom temperature of the snow cover, BTS, temperature loggers, geophysical methods and geomorphologic mapping). This study focused mainly on the demonstration of the possibilities offered by multitemporal ALS data for the detection of local patterns of permafrost distribution in an alpine area.

Therefore the aim of this project was to on i) detect locations where melting of permafrost leads to geomorphologic changes with the use of high resolution data (especially ALS and aerial photogrammetry) and ii) to provide a (operational) methodology for on-going, spatially continuous, area-wide monitoring of geomorphological significant permafrost change.

2 Study sites

2.1 Äußeres Hochebenkar (AHK)

Hochebenkar rock glacier (46° 50’ N, 11° 00’ E) is a tongue-shaped, talus derived rock glacier about 2 km south of Obergurgl (Ötztal Alps, Austria). It expands from about 2,830 m a. s. l. down to about 2,360 m a. s. l. and reaches a length of 1.1 km

at its orographic left, and up to 1.6 km at its orographic right side. A detailed characterisation of the physiognomy of AHK is given by Vietoris (1972) and Haeberli & Patzelt (1982). Since 1938 (Pillewizer 1957) systematic terrestrial investigations on surface flow velocities, front advance rates and surface elevation changes of AHK have been carried out on an annual scale (Schneider & Schneider 2001). Remote sensing methods, like terrestrial and aerial photogrammetry have been applied additionally (Kaufmann & Ladstädter 2002, 2003).

The AHK is characterised by very high surface velocities of up to several meters per year. According to Schneider and Schneider (2001) maximum displacement rates (6.6 m / a) were measured below a terrain edge at about 2,570 m a. s. l. between the 1950 / 60s. Following Haeberli & Patzelt (1982), these high values are most likely a result of a significant increase of slope steepness below the terrain edge. The related velocity gradients express themselves in deep cross cracks in the rock glacier body (Schneider & Schneider 2001).

2.2 Reichenkar (RK)

Reichenkar rock glacier (47° 02' N, 11° 01' E) is located in the western Stubai Alps (Tyrol, Austria). It is situated in a small, northeast-facing valley called Inneres Reichenkar, which connects to a larger valley, the Sulztal, in the western Stubai Alps. RK is a tongue-shaped, ice cored rock glacier, 1,400 m long with widths that reach 260 m near the head and 170 to 190 m near the front. The rock glacier covers an area of 0.27 km^2 and extends from 2,750 m to an altitude of 2,310 m. The front slope has a steep gradient of 40–41°.

Detailed information about this rock glacier can be found in Krainer & Mostler (2000, 2002), Krainer et al. (2002) and Hausmann et al. (2007). Investigations on surface flow velocities have been carried out in the period 1997 to 2003 with differential Global Positioning System (dGPS) measurements (Chiesi et al. 2003). These data are used to validate the derived horizontal displacement rates. The dGPS measurements were acquired along seven cross profiles at RK with 36 measured points (Krainer & Mostler 2006).

2.3 Schrankar (SK)

The rock glaciers of the Schrankar (47° 03' N, 11° 05' E) are located in the Western Stubai Alps (Tyrol, Austria) in a north to south aligned valley. There are up to 12 rock glaciers of different activities between elevations of 2,400 and 2,800 m a. s. l.. Due to the different activity states, the slope angles of the fronts vary between 32° and 43°. Additionally, beside the rock glaciers, a big dead ice body below the terrain edge of the southern Schrankarferner was identified. Unfortunately, there are no historical surface velocity measurements.

2.4 Ölgrube (OGR)

The rock glacier Ölgrube (46° 53' N, 10° 45' E) is in a small east-west trending site valley of the Kauntertal valley and lies in the western margin of the Ötztaler Alps. Ölgrube consists of two adjacent tongue shaped rock glaciers with different activities and different spatial origins. Although they are separated by a middle moraine, they appear as on rock glacier. It has spatial distribution of 880 m length and 250 width and lies between 2,800 and 2,380 m a. s. l.. The rock glacier has a remarkable front with 60 m height and a slope angle of 38°. The first surface velocity measurements were carried out by Finsterwalder (1928) and Pillewizer (1939), and later on between 2000 and 2005 (Berger et al. 2006; Krainer & Mostler 2006 and Hausmann et al. 2007).

2.5 Rofenberg

The study area Rofenberg (46° 58' N, 10° 48' E) in the Ötztal Alps (Austria) can be characterized as a typical high Alpine environment in mid-latitudes, which ranges between approximately 2,800 and 3,229 m a. s. l.. Areas that were not covered by Little Ice Age (LIA) glaciers have been exposed to permafrost friendly conditions. However, these areas are well suited for investigations aiming the detection of permafrost evidence with a combination of methods (see section 4.4).

2.6 Montafon

The study area Montafon is a 40 km long valley in Austria (Federal State of Vorarlberg), which ranges from the Bielerhöhe to the city of Bludenz to the Silvretta mountain range (see Fig. 13). The valley is surrounded by the Verwall group in the north and the Rätikon and Silvretta group in the south. The highest peak is the Piz Buin (3,312 m a. s. l.) in the Silvretta group. The quantification of vertical and horizontal surface changes in the Montafon Range based on ALS data was one major objective during the last project year. The workflow established on the above mentioned rock glaciers could be successful adapted to the new ALS data from the area of Montafon (Vorarlberg) and the derivation of surface changes, which have been done on these single rock glaciers could be applied for the whole region to detect area wide surface changes.

3 Data

For each of these study sites presented above, basic ALS information is available. These data include at least the coordinates (x, y and z). In exceptional cases additional information about the reflectance of the surface (so called intensity information) are

available. Terrain and surface information are separated, resulting in digital terrain models (DTMs), which are significant for the area wide permafrost ALS analysis.

In the year 2006, the relevant part of the Stubai and Ötztal Alps were captured by ALS campaigns, ordered by the Tyrolean Government. The Montafon Range was measured with ALS in 2005 (on behalf of the Government of Vorarlberg). To reach the objectives of the project the introduction of a multi-temporal component in terms of ALS is necessary. For that purpose and in addition to the basic ALS information supplementary ALS information are required. At the Institute of Geography various ALS campaigns have been carried out in the Tyrolean Alps during the last decade. Some of these data are supported to the permAfrost project. ALS data acquisition campaigns at AHK, RK, SK and OGR have been carried out in 2009 and 2010. The 2009 data was acquired within the research project C4AUSTRIA (Climate change consequences on cryosphere, funded by the Austrian Climate Research Programme ACRP), the 2010 data within the MUSICALS project (alps – Centre for Climate Change Adaption Technologies). Additionally, at RK a flight campaign has been carried out in 2007 by the Institute of Geography. The team obtained the permission for the usage of these data in the permAfrost project in order to investigate area-wide geomorphological significant permafrost change. A summary on the exact data acquisition dates is given in Bollman et al. (2011). Table 1 gives an overview of the ALS data, which were used in the permAfrost project. All ALS data have been stored in a Laser Information System (LIS). LIS is able to store and handle ALS point data as well as raster data and is an excellent multi-user environment. Furthermore, the system opens the opportunity to enhance or develop ALS analysis tools.

The ALS campaign for the Montafon Range was organized by the Institute of Geography in the framework of the permAfrost project in autumn 2010. Bad weather conditions (snow fall in higher regions) made it impossible to finish the entire area. Figure 2 gives an overview of the measured flight trajectories in the Montafon

Table 1: ALS data for the analysis of permafrost changes; [1) 2)] entire areas – organized by the Goverments of Tyrol and Vorarlberg; [3)] Reichenkar; [4) 5)] Reichenkar, Schrankar, Hochebenkar, Ölgrube; [6)] permAfrost ALS flight campaign Montafon; [7)] Reichenkar (not used 2011)

Region	2005/2006	2007	2009	2010	2011
Stubai Alps	x [1)]	x [3)]	x [4)]	x [5)]	x [7)]
Ötztal Alps	x [1)]		x [4)]	x [5)]	x [7)]
Montafon Range	x [2)]			x [6)]	

Table 2: Minimum point density

Region	2005 / 2006	2007	2009	2010	2011
Stubai Alps	1 pt / 4 m²	2 pts / m²	2 pts / m²	2 pts / m²	2 pts / m²
Ötztal Alps	1 pt / 4 m²		2 pts / m²	2 pts / m²	3 pts / m²
Montafon Range	1 pt / m²			2 pts / m²	4 pts / m²

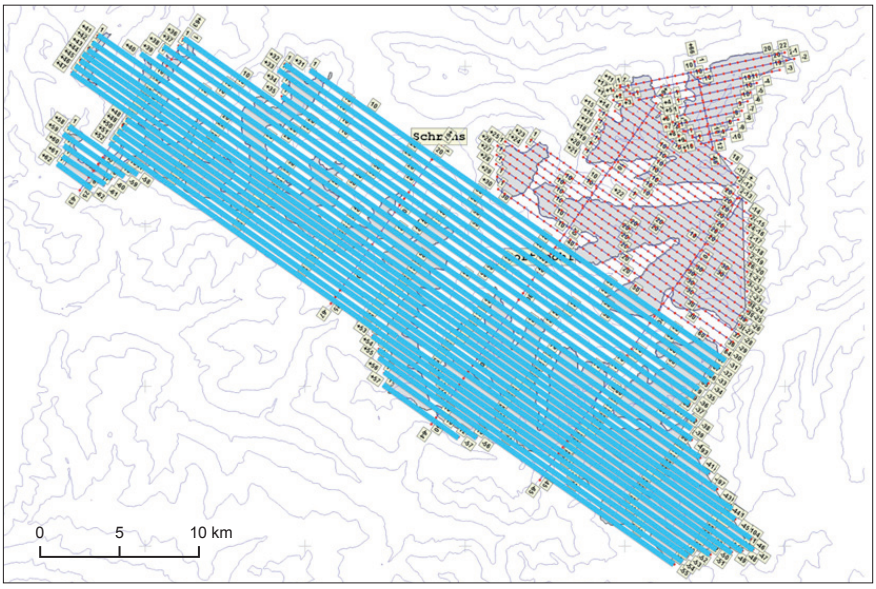

Figure 2: Flight plan and trajectories acquired in autumn 2010 (blue) and in autumn 2011 (red), Montafon Range

Range in 2010 (blue). The northern part has been measured in autumn 2011. Compared to the point density of the first flight campaign in 2010, the laser scanning data has been ordered with a point density of at least 4 pts / m² (cf. Table 2).

The higher point density and the expansion of the flight area were enabled by an agreement between the Institute of Geography, University of Innsbruck and the Landesvermessungsamt Vorarlberg (department VoGIS).

Additionally to the flight campaign of the Montafon, on 6 November 2011 a GPS campaign was carried out to support the company TopScan with GPS reference data, which will be used to georeference the ALS raw data. 72 GPS points were measured in the south-eastern part of the Montafon Range close to Silvretta lake (Bieler Höhe, Silvretta group) with an average accuracy (x, y and z) of approximately 10 to 17 cm.

3.1 ALS data quality control and data processing

In general the data point cloud data (x, y, z and intensity). As mentioned above, data are stored in the LIS data base. In case of permAfrost a filtering of first or last pulse was, due to the absence of higher vegetation (trees, scrubs) in permafrost terrain, not necessary.

The ALS data quality control is an important step in the ALS based permafrost analysis work flow. The quality control of the archive (2005 / 2006, 2007, 2009 and 2010) data has been done within the framework of relevant projects (e. g. C4AUSTRIA, MUSICALS). The quality control of the ALS campaign Montafon has been

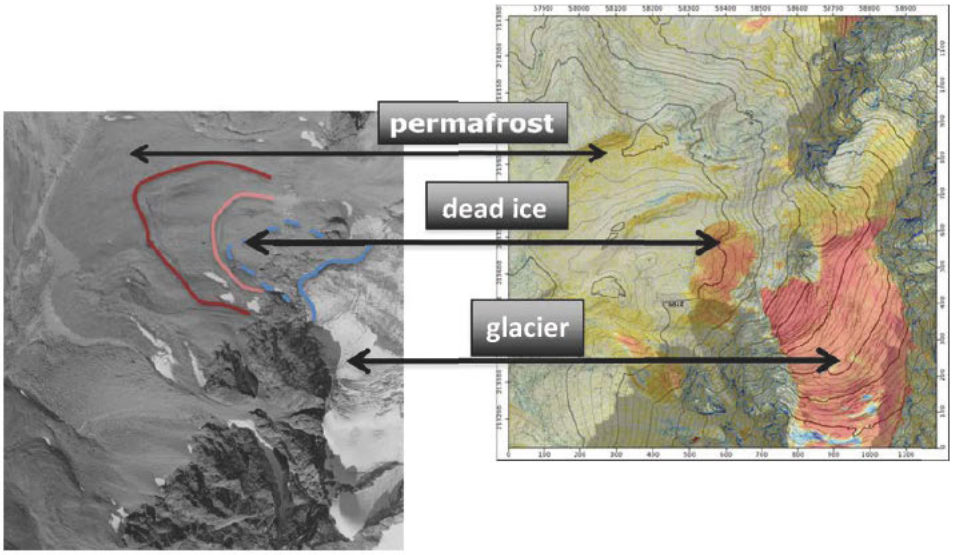

Figure 3: Part of SK, combination of various remote sensing methods and mapping of various cryospheric processes (glacier dynamic, dead ice development and permafrost) calculated by differencing ALS data

done immediately after data delivery. Particular efforts have been undertaken to improve existing data sets and in particular to check the quality of the Montafon ALS data The first part of the study aimed at quantifying the vertical accuracy of the available multi-temporal ALS data sets In comparison with differential dGPS measurements the vertical accuracy of the ALS point data is in the range of ±0 10 m (mean absolute error), with a standard deviation of ±0.10 m for relatively flat and homogeneous areas. Including point to raster aggregation errors as well, the cumulative errors (e. g. <0.12 cm in 40° steep and rough terrain) are also promising. Hence, surface elevation changes which exceed these error margins can be assigned to permafrost related activities.

On base of these point data DTMs were calculated using different algorithms and settings. Good results were achieved with cell sizes down to 1 m, or even down to 0.5 m, if gaps were closed. DTM from different years have been used to analyse volume changes and to create a surface changes map by simply differencing the DTMs. It is obvious that ALS is able to deliver information about terrain and changes therein where, due to shadow effects, no information are available in orthoimages (Fig. 3).

Figure 3 gives an impression of how data from two ALS campaigns are combined to get information about altitudinal changes in an Alpine terrain. It captures the entire Schrankar area and shows the altitudinal changes corresponding to cryospheric processes between 2006 and 2009. Large changes can be observed in glaciated areas, moderate changes in dead ice areas and where debris flows occurred and small changes where permafrost melting is assumed. The know-how for the data handling, the quality control and the co-registration have been acquired at the Institute of Geogra-

phy during various ALS related projects (e. g. C4AUSTRIA (Climate Change Consequences on the Cryosphere), Austrian Climate Research Program), which lead to synergistic effects (application of already developed tools or improvement of existing tools for example) across the linked projects.

4 Project related activities

4.1 Quantifying surface changes on rock glaciers: Photogrammetric and ALS measurements

The quantification of vertical and horizontal surface changes based on ALS data was one major objective within the second project year. These calculations are useful in order to get more exact information about the response of permafrost phenomena to the process of climate change and build an important analytical component for permafrost distribution mapping, because it allows identifying the state of activity of rock glaciers. Within this objective we reconstructed and analysed the surface displacements on four rock glaciers in the Stubai and Ötztal Alps. These results are derived from aerial images and ALS data over the period 1953 / 54 to 2011. Using ALS data in rock glacier research, especially for validating the photogrammetric derived DEMs, and for calculating flow velocities is an innovative method for area-wide investigations on permafrost.

4.1.1 Data

The basic data applied in the analysis are on the one hand greyscale aerial photographs, provided by the Austrian Federal Office of Metrology and Survey (BEV), with a scale from 1 : 16,000 to 1 : 30,000. For the study sites, analogue aerial stereoscopic pairs were available for the years 1953 / 54, 1969, 1971, 1973, 1977, 1989, 1990, 1994 and 1997, taken with Wild / Leica-Cameras of different types. Additionally, the federal province of Tyrol provided high resolution orthoimages from the years 2003 and 2009.

To pursue the objective target at best, the date of recording is very important, because the objects of interest are situated at around 2,300–2,900 m a. s. l, and snow-covered areas would make DEM generation impossible. Another problem concerning DEM generation is the topographic shadowing effects. For that reason, only aerial photographs with a certain standard were used.

On the other hand ALS data were applied, which have been acquired in flight campaigns at AHK, RK, SK and OGR in 2006, 2009, 2010 and 2011. The 2006 campaign was initiated by the federal province of Tyrol. As mentioned above, the 2009 and 2011 data were acquired within the C4AUSTRIA, the 2010 data within the MUSICALS project. DEMs out of these ALS flight campaigns were generated and integrated in the analysis. Additionally, at RK a flight campaign has been carried out in 2007.

4.1.2 Method

For the photogrammetric analyses the analogue data were provided by BEV as scanned aerial photographs (ca. 1,600 dpi). Additionally the required calibration reports were supplied. Image orientation, automatic DEM extraction and digital orthophoto generation were performed within the application LPS of the software ERDAS, as well as the application OrthoEngine of the software Geomatica.

For detailed description of the method see Baltsavias (2001), Kääb (2004) and Kraus (2004). The DEMs were generated from the mono-temporal stereo-models with 1 m spacing. Additionally, the orthoimages were calculated with the resampling-method cubic convolution and with 0.2 m ground resolution.

Afterwards an accuracy assessment is performed by comparing the generated DEM, especially with the high-quality DEM of the ALS flight campaign of 2009. Therefore three areas are detected, which represent the surface structure (slope, aspect, height) of the rock glaciers but are located in stable regions. On the basis of this analysis the root mean square error (RMSE) could be calculated. The computed RMSE for AHK, RK, SK and OGR (cf. Table 3) show values of 0.2–1.3 m. Afterwards the vertical changes were derived through subtraction of the multitemporal DEMs over the different periods.

The horizontal displacement rates out of the orthoimages were calculated with the Correlation Image Analysis (CIAS) Software (Kääb & Vollmer 2000). CIAS identifies displacement rates as a double cross-correlation function based on the grey values of the used input images (Kääb 2010). The correlation algorithm searches via block matching a predefined corresponding reference section in the image of acquisition time 1 (t_1) in a sub-area of image of acquisition time 2 (t_2). For measuring changes in

Table 3: Calculated RMSE for the generated DEM vs. ALS DEM 2009. (–) Aerial images not available or acquisition in winter

DEM	RK-RMSE	AHK-RMSE	SK-RMSE	OGR-RMSE
2011 (ALS)	0.10 m	0.11 m	0.12 m	0.09 m
2010 (ALS)	0.11 m	0.12 m	0.11 m	0.13 m
2009 (ref. ALS)	ref	ref	ref	ref
2006 (ALS)	0.13 m	0.10 m	0.12 m	0.11 m
1997	–	0.41 m	–	
1994	0.22 m	–	0.32 m	
1989 /1990	0.26 m	0.42 m		
1977	–	0.25 m	–	–
1973	1.29 m	–	0.64 m	0.83 m
1971	–	0.55 m		–
1969	–	0.29 m	0.42 m	–
1953 / 1954	0.78 m	0.58 m	0.63 m	0.55 m

geometry, relative accuracy is more important than the absolute position of the images (Kääb 2002). Therefore, the multitemporal orthoimages have been co-registered using tie points in addition to the initial georeferencing.

Additionally the horizontal displacement rates are calculated from shaded reliefs of ALS DEM with the open source image correlation software Imcorr (Scambos et al. 1992), which applies also digital matching techniques using normalized cross-correlation (NCC) to calculate flow velocities (Scambos et al. 1999).

The accuracy of the calculated horizontal displacement rates on AHK based on ALS DEM is evaluated using dGPS data. As the dGPS measurements and ALS data acquisitions have not been carried out at the same dates, the ALS based displacement rates are adjusted to the time span between the dGPS data acquisitions using

$$\overline{dALS_{t1,t2}} = ALS_{t1,t2} / \Delta tALS_{t1,t2} \cdot \Delta tdGPS_{t1,t2} \quad (1)$$

where $\overline{dALS_{t1,t2}}$ is the adjusted displacement rate [m / a] of the Imcorr results, $ALS_{t1,t2}$ is the displacement rate of the original Imcorr results, $\Delta tALS_{t1,t2}$ is the number of days between the ALS flight campaigns and $\Delta tdGPS_{t1,t2}$ is the number of days between the dGPS measurements (Bollmann et al. 2012). The time adjusted Imcorr output point file as well as the interpolated displacement raster values are compared to the dGPS displacement rates. For the generation of displacement grids a trimmed mean interpolation function (search radius 2 m) was used. This allowed the removal of erroneous measurements (outliers) (cf. Bollmann et al. 2012). For the 2009 / 2010 time period 39 dGPS measurements from the cross profiles *L0* to *L3* are used for validation. For the period 2006 / 2010 dGNSS data from *L1* is not available, therefore

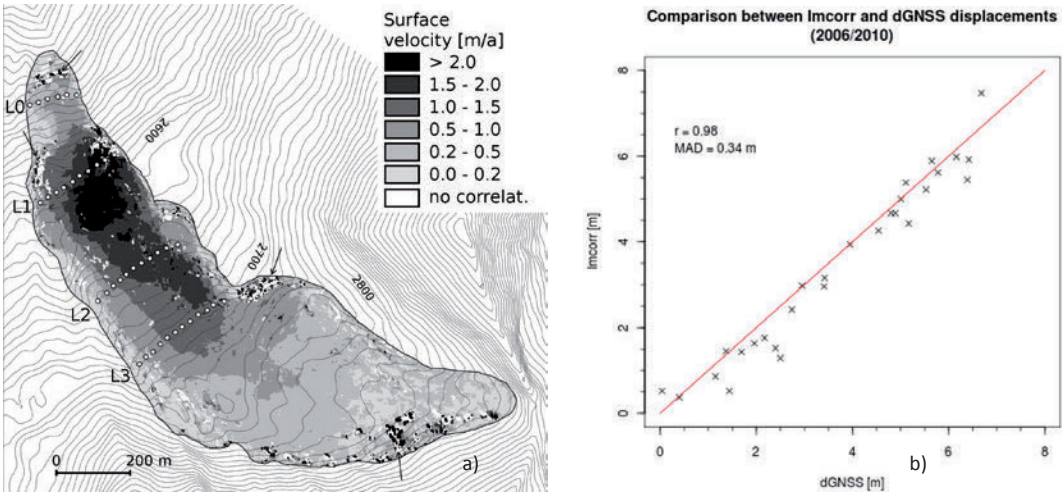

Figure 4: a) Mean annual surface velocity of AHK between 2006 and 2010. Results interpolated from Imcorr output. L0 to L3 (white circles) indicate location of dGPS measurement points along 4 cross profiles. Arrows indicate areas with artifacts. b) Comparison between Imcorr and dGPS displacements on AHK between 2006 and 2010

Table 4: Comparison between horizontal displacement rates calculated from CIAS (orthoimages) and Imcorr (ALS-data) with dGPS (Imcorr – dGPS) for the periods 1997–2003, 2006–2010 and 2009/2010. In columns with "Pts." to original CIAS/Imcorr output points are compared to dGPS, otherwise the interpolated rasters

CIAS / Imcorr – dGPS	mean [m]	abs.mean [m]	std [m]	max [m]	min [m]	RMSE [m]	R^2
OP CIAS Pts. 1997-2003	0.24	0.4	0.46	1.28	0.02	2.05	0.91
ALS Imcorr Pts. 09-10	0.09	0.28	0.50	2.50	0.66	0.50	–
Raster 09-10	0.06	0.27	0.48	2.42	0.69	0.47	0.98*
Pts. 06-10	0.50	0.68	3.57	18.6	1.02	3.54	–
Raster 06-10	-0.25	0.28	0.44	0.80	1.22	0.50	0.94*

only 28 reference measurements could be used (see Fig. 4a, b). The vertical accuracy of the generated DTMs at AHK is determined using eleven dGPS measurement sites. The eleven fix points are not influenced by any topographic changes.

Furthermore the results of RK based on orthoimages were compared with measured dGPS flow velocities. The original CIAS output point files, as well as the automatically measured displacement vector values, were compared to the dGPS displacement rates, using a buffer of 3 m around the dGPS points. Table 4 presents the calculated differences by CIAS and Imcorr, considering the mean absolute error (*abs. mean*) in combination with the standard deviation (*std*) to be the most appropriate accuracy indicators.

For the time period 1997–2003, an absolute mean deviation of 0.4 m (*std* 0.46 m) between the dGPS values and the corresponding nearest CIAS point measurements was calculated. Figure 4b shows the computed and the 36 dGPS measured flow velocities within the investigated periods (cf. Fig. 5a, b). Additionally, the dGPS points were used as reference for the periods 1954–1973 and 2003–2009. In contrast to the latter epoch, the velocities between 1954 and 1973 were slower in evidence, but there is still a good relative correlation within the profiles.

4.1.3 Results and Interpretation

In the case of RK, AHK and OGR permafrost creep is the most important factor governing surface elevation changes. Additionally, the derived high annual mean velocities on RK revealed further processes, which could be involved in surface displacement. Horizontal and vertical displacements of RK, AHK, SK and OGR could be successfully calculated from multitemporal aerial photographs and ALS data over a period of 57 years. The existing knowledge about the flow behavior of the three rock glaciers could be confirmed with the method and reconstructed. Furthermore the length of the time series allowed the investigation of temporal variations in flow velocities, which has little been done for a fast flowing type like RK or AHK. The study revealed an acceleration of the investigated rock glaciers since the late 1990s (cf. Table 5). In the following the results of RK and AHK will be presented in detail, whereas some results of OGR and SK will be presented as figures (cf. Fig. 9 and 10).

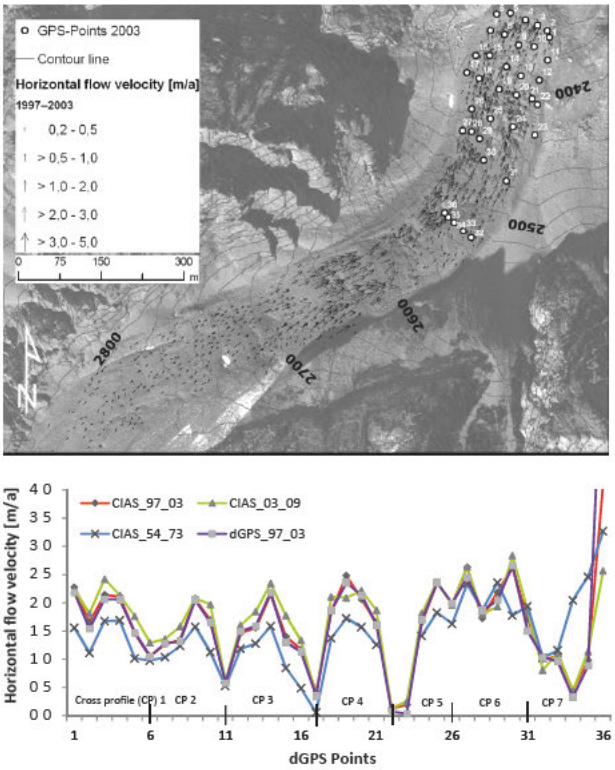

Figure 5: a) Mean annual horizontal flow velocity on RK between 1954–1973. White circles indicate location of dGPS measurement points along 7 cross profiles. b) Comparison of the measured (dGPS) and computed (CIAS) flow velocities for periods 1997–2003, 2003–2009 and 1954–1973

In contrast to AHK, where the displacement rates have been similar to nowadays in the 1950s and 1960s, the RK shows acceleration over all periods from 0.75 to 1.3 m / a nowadays. Beside the temporal variation, also a spatial variation in the velocity field of RK could be detected. So it seems that the orographic left part of the rock glacier in the middle and lower section show higher velocities.

4.1.3.1 Reichenkar

The horizontal surface velocities and the thickness changes on RK (cf. Fig. 6) varied between the individual investigated epochs. From 1954–2011 an average vertical loss of the rock glacier of nearly 3.2 m (ca. –6 cm/a) can be observed. In the rooting zone surface lowering of up to –0.5 m/a in various periods indicates massive loss of ice. The average elevation change in this zone lies within the range of –0.10 m/a.

The increase in thickness at the front of individual flow lobes suggested that elevation changes are influenced by mass advection. Over the investigated periods, the surface of RK was creeping with average rates of 0.9 m / a (cf. Table 5). Maximum creep rates occur in a transition zone (2,540–2,660 m a. s. l.), a steeper mid-section before the flat tongue, where compressive flow with development of transverse ridges and furrows can be observed. The measured surface displacements depict acceleration since the late 1990s, from the middle to the front part of the rock glacier. The

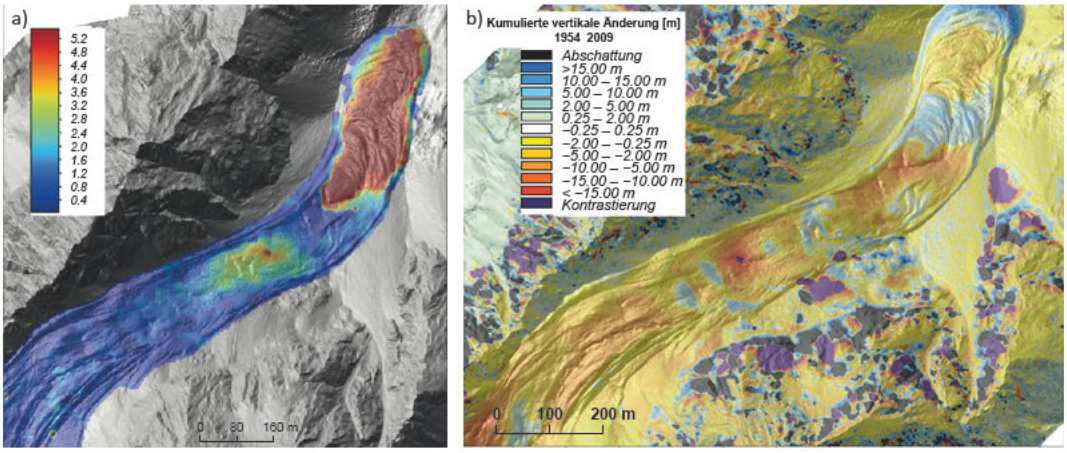

Figure 6: a) Displacement field (unclassified) of RK derived from generated DEM based on ALS data (time 1: 30 September 2009, time 2: 7 October 2010). Ground resolution was 50 cm. 6736 homologous points were matched on RK. b) Difference image of RK, calculated by differencing DEM of 1954 generated from aerial images and ALS data from 2009. Black and purple areas indicate errors because of bad contrast or shadowing effects.

displacement rates in the root zone seem to be constant over the whole period (0.2–0.5 m / a), whereas flow rates at the tongue, which were consistent over the periods from 1954–1997 with average rates of 1–2 m / a along the central axis, increased to 2–3 m / a since 1997. The increasing velocities cannot be explained by the gradient of the slope, which measures only 11–12° on the lower part of RK.

The front of RK advanced 53 m from 1954 to 2009 (0.76 m / a). Figure 7 depicts the mentioned acceleration, which increased from an average of 0.6–1.55 m / a during the last 20 years. The measurements show highest displacement rates at the front

Table 5: Calculated horizontal velocity from orthoimages with CIAS (mean, maximum velocity & acceleration dv) of all periods on RK and AHK. The two rock glaciers were separated into three sections (root zone, transition zone and tongue), in every sector the same amount of measured blocks was used for calculation of the annual mean (cf. Klug et al. 2012)

Period	Measured blocks	Mean velocity [m/a]	Max. velocity [m/a]	dv [%]
Reichenkar				
1954–1973	841	0.75	3.4	–
1973–1989	871	0.73	3.5	–2.7
1989–1994	909	0.73	4.2	0.0
1994–1997	987	0.76	5	+ 3.2
1997–2003	830	1.12	4.9	+ 47.4
2003–2009	811	1.3	4.1	+ 16.1
Hochebenkar				
1953–1969	2438	0.84	5.2	–

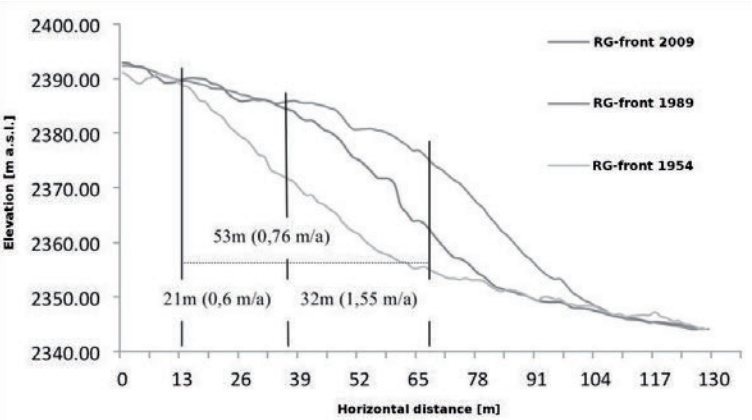

Figure 7: Front advance depicted by longitudinal profiles

within the range of up to 3 m / a. At the orographic left part of the flat tongue (2,520–2,460 m a. s. l.), one part features relatively high movement rates (ca. 3.3 m / a) since 1994. In combination with the general topography the distinct velocity gradients indicate that the lower part of the frozen body is overridden from above by a new lobe (Klug et al. 2012).

On the base of the calculated vertical changes and the different delineated areas it was tried to derive the balance of the rock glacier RK and to calculate the water equivalent. The difference grids have been separated in positive and negative values, whereat areas representing errors caused by bad contrast or shadowing effects in photogrammetrical derived differences have been excluded. The mean annual *dz* integrated over the rock glacier area amounts to –5.6 cm / a. By multiplying the calculated *dz* with the density of ice (900 kg m^{-3}) the water equivalent has been calculated, which amounts to a mean annual loss of –58.3 mm w. e. (cf. Table 6).

Table 6: Mass balances on RK

Period	Mass gain [m³]	Mass loss [m³]	Balance [m³]	m³ / a	dz / a [m]	mm w. e. / a
1954–2011	209,908	1,188,932	–979,024	–17,175.9	–0.064	–58.3
1954–1973	60,403	348,471	–288,068	–16,945.2	–0.063	–51.5
1973–1989	58,167	331,322	–273,155	–15,175.3	–0.056	–58.0
1989–1994	23,856	88,347	–64,491	–12,898.2	–0.048	–43.8
1994–2006	44,309	247,332	–203,023	–16,918.6	–0.063	–57.5
2006–2009	34,945	80,848	–45,903	–15,301.0	–0.057	–52.0
2006–2007	24,396	33,922	–9,526	–9,526.0	–0.035	–32.4
2007–2009	28,259	62,181	–33,922	–16,961.0	–0.063	–57.6
2009–2010	33,470	50,728	–17,258	–17,258.0	–0.064	–58.6
2010–2011	27,353	42,496	–15,143	–15,143.0	–0.056	–51.4

4.1.3.2 Hochebenkar

The rock glacier is characterized by a comparatively high flow velocity of several metres per year and periodically changing flow rates between 1953 and 2011 (cf. Table 5). A transverse terrain edge at an altitude of about 2,580 m a. s. l. divides the rock glacier into a lower steep part and an upper flat part. Within all periods, the rooting zone shows constant velocities (0.2–0.5 m / a), whereas in the adjacent zone towards the terrain edge displacement rates differ during the investigation periods.

In the period from 1953 to 1969, high movement rates (1.0–2.5 m / a) were measured in this zone. At the same time, the upper part of the tongue showed the development of massive transverse cracks, where the loss of mass was extremely high. From the early 1970s to the beginning 1990s, a phase with relatively slow average annual velocity rates (0.5–1.0 m / a, Table 3) could be shown. From the 1990s onwards, the movement rates increased, showing velocities (1.0 to 2.5 m / a) similar to that of the late 1960s (Fig. 8). On the terrain edge, creep velocities increased to about 2.5 m / a. Maximum creep rates (6.9 m / a) have been measured in this transition zone from 1953 to 1969, although rockfall may be a significant process here and cannot be attributed to permafrost creep exactly.

Surface elevation change rates > 5 m are identified in several areas of AHK. At the orographic right margin of the rock glacier values > 0.5 m are caused by creep processes that resulted in a downward transport of mass and expansion of AHK between 2006 and 2010 (Fig. 11). Distinct elongate-shaped alterations of positive and negative values occur on the main part of the rock glacier, especially between 2,730 and 2,820 m at the orographic right side. They clearly result from advancing ridges and furrows. Between *L0* and *L1*, at about 2,500 m at the middle part of AHK, a sharp

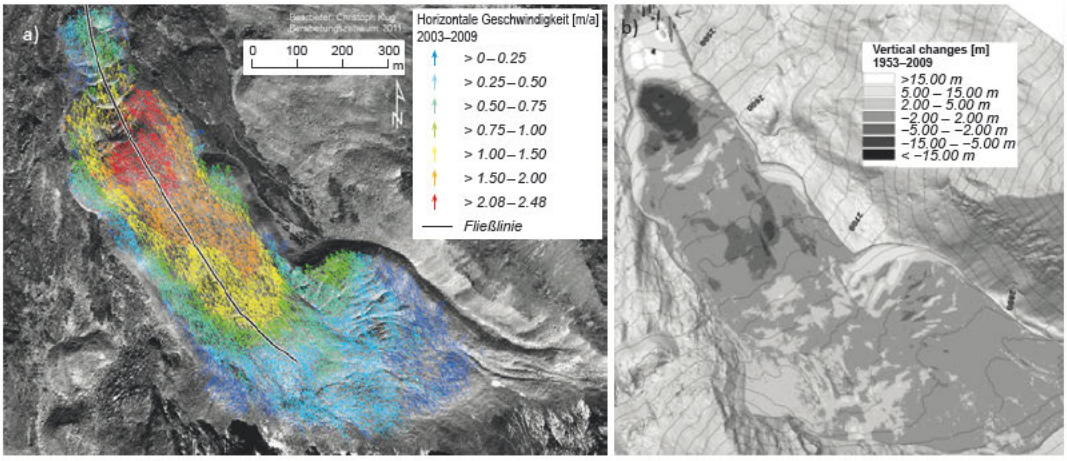

Figure 8: a) Displacement vectors of AHK derived from generated orthoimages (time 1: 9 September 2003, time 2: 18 September 2009). Ground resolution was 20 cm. 2,439 homologous blocks were successfully matched using CIAS. b) Cumulated vertical changes of AHK between 1953 and 2009. Arrow at the front indicates errors because of bad contrast

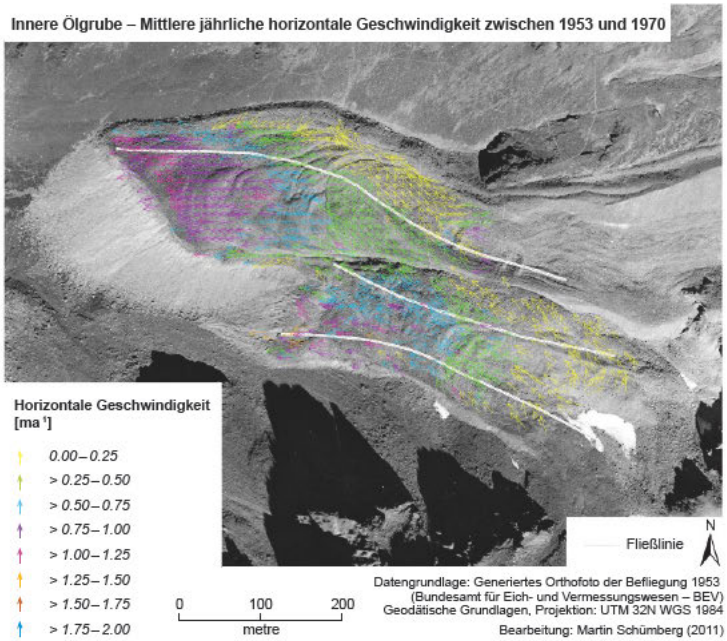

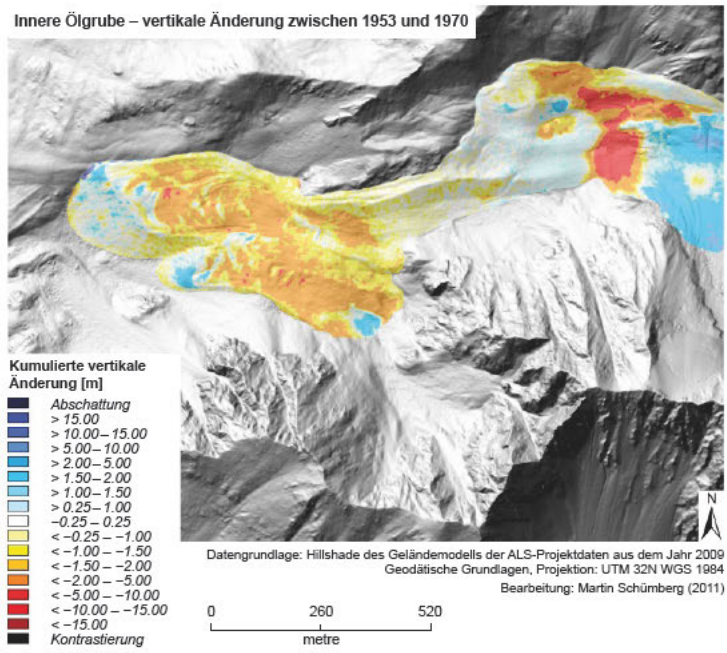

Figure 9: above – Displacement vectors of OGR derived from generated orthoimages (time 1: September, 1953, time 2: 29 September 1970). Ground resolution was 20 cm. 2,149 homologous blocks were successfully matched using CIAS. below – Cumulated vertical changes of OGR between 1953 and 1970

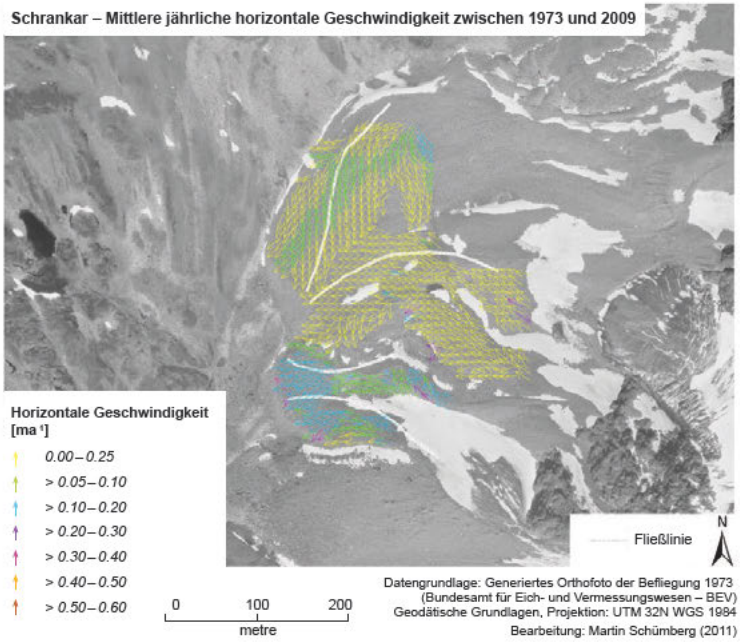

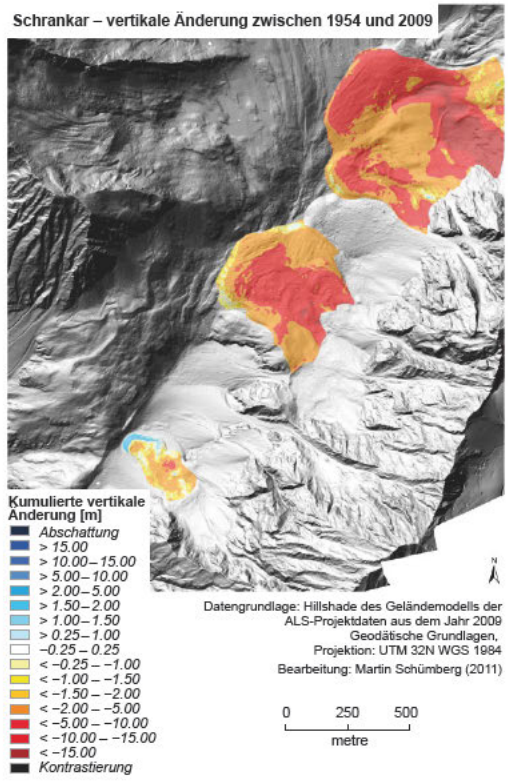

Figure 10: above – Example of displacement vectors of SK derived from generated orthoimages (time 1: September, 1973, time 2: 29 September 2009). Ground resolution was 20 cm. 2,149 homologous blocks were successfully matched using CIAS. Below – Cumulated vertical changes of SK between 1954 and 2009

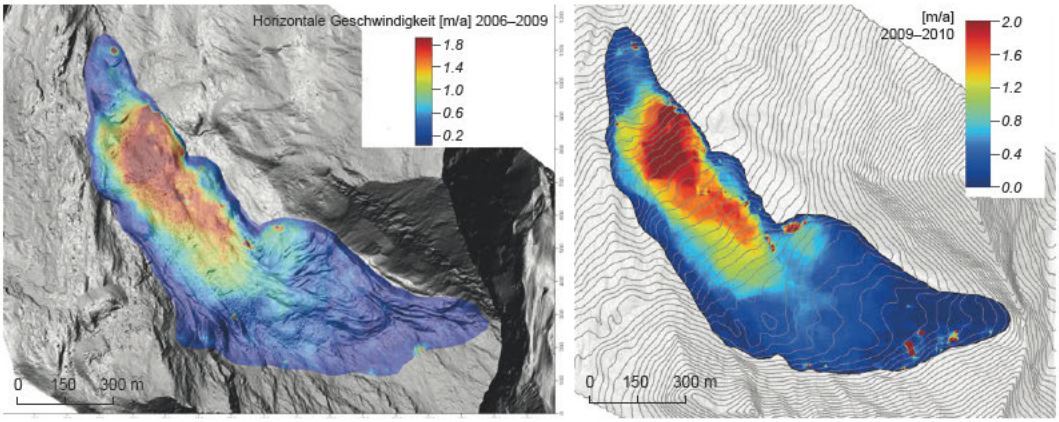

Figure 11: Displacement field (unclassified) of AHK derived from generated DEM based on ALS data (time 1: 18 September 2006; time 2: 30 September 2009). Ground resolution was 50 cm. 7,751 homologous points were successfully matched using Imcorr (left). Displacement field (unclassified) of AHK (time 1: 30 September 2009, time 2: 7 October 2010). Ground resolution was 50 cm. 7,912 homologous points were successfully matched using Imcorr on AHK (right)

transition from areas with high surface elevation decrease and gain is evident. These areas correspond well with the area described by Haeberli & Patzelt (1982) and Schneider & Schneider (2001) where deep cross cracks occur as a consequence of local sliding of the rock glacier on the bedrock and increased tension in the permafrost body.

In the upper part the measurements show elevation changes within the range of –0.10 m / a, whereas the changes increase to nearly –0.6 m / a at the zone below the terrain edge (Fig. 12). Thinning of the frozen debris at the terrain edge of around 2,580 m a. s. l. is compensated to a large extent by corresponding thickening in the lowest part. Below 2,580 m, which marks the end of the steady-state creeping zone, the tongue has moved into very steep terrain. In this area landslides have occurred due to the specific topographic situation and make image correlation nearly impossible. The front of AHK advanced from 1953 to 2011 135 m (2.4 m / a). Since 1969 the rates of front advance decreased from 4.1 m / a to 1 m / a in the 1990s, since that time an increase could be observed to 1.6 m / a nowadays.

In general, the detected local surface elevation changes of AHK are caused by horizontal displacements of the creeping rock glacier. Regarding the whole rock glacier, an area-averaged mass loss is not detected. Therefore, the ice content of AHK seems to be well protected from surface energy input and significant ice melt did not occur between the investigated periods.

In a detailed investigation of the ALS data 2006, 2009 and 2010 of AHK, individual surface velocity fields have been detected for the time period 2006 to 2010 (Fig. 11). In general, the mean annual velocity increases gradually from < 0.2 m / a at the root zone to a maximum of > 2 m / a in the middle part of the rock glacier and at its orographic right side at about 2,600 m a. s. l..

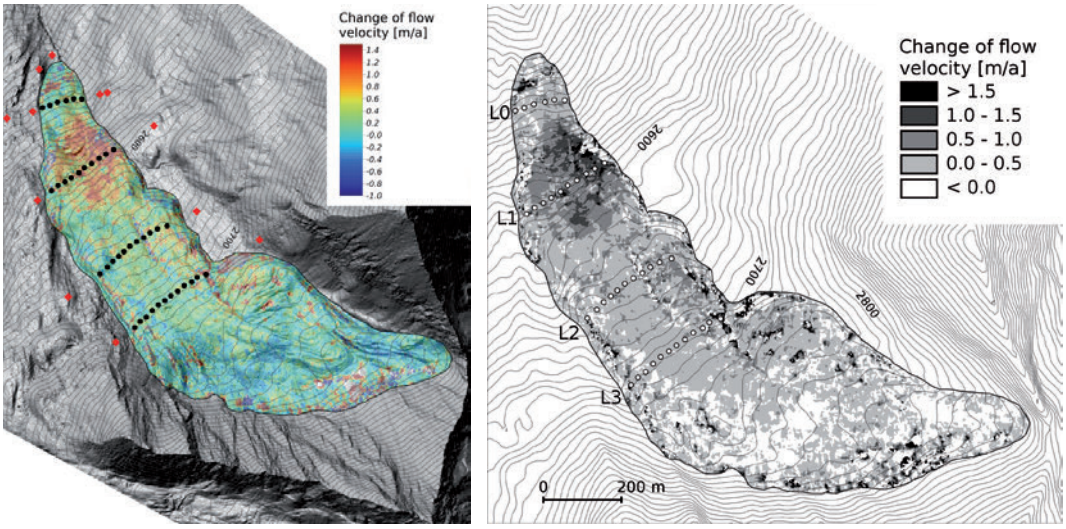

Figure 12: Changes in mean annual flow velocity unclassified (above) and classified (below) between the time period 2006/2009 and 2009/2010

Maximum velocities correspond well with an increase of terrain steepness below 2,640 m. Below 2,560 m the surface velocity decreases again, even though the terrain is still steep. A complete decoupling of the upper and lower part of AHK, as has been assumed by Haeberli & Patzelt (1982), cannot be found in the analysis of the 2006 to 2010 velocity fields. The velocity decrease between *L1* to *L0* is rather gradually than abrupt. However, the lowest part of AHK (around *L0*) is clearly influenced by other creep characteristics than the part above 2,560 m (Fig. 12).

For some areas no creep rates could be calculated, because no correlations between the two input images are made by Imcorr. These areas either occur at steep lateral sides or in fast creep steep areas. In these areas the surface topography changes strongly due to rotation of boulders and surface instabilities. Several velocity artifacts (arrows in Fig. 8), resulting from miss-matching of the two Imcorr input images occur. In most cases, they are spatially connected to areas where no correlation of the two images could be made. Such areas have to be excluded from interpretation.

Between the period 2006/2009 and 2009/2010 a general velocity increase is detected. Comparing Figure 12 left and right shows, that the absolute increase of surface velocity is highest for areas that initially show high mean annual velocities. The most significant acceleration in the order of 1.0–1.5 m/a occurs in the steep part of the rock glacier at the cross profile line *L1*. Velocity changes in that area have been discussed by Haeberli & Patzelt (1982) and Schneider & Schneider (2001).

Most likely, they do not present variations in internal creep characteristics, but are a result of sliding at the base of the creeping permafrost body on the bedrock. Over large parts of the rock glacier, a velocity increase in the order of 0.0–0.5 m/a is observed, whereas towards the root zone slightly negative values are calculated. These

values are close or below to the level of significance of 0.3 m (cf. Table 4; *std* raster 09 / 10). Thus, considering the accuracy of the data and method, it cannot be state that the velocity really decreased in the root zone of AHK.

4.1.4 Conclusion

Although it is impossible to derive the flow mechanics of a rock glacier from its measured velocities, some conclusions may be drawn out of the area-wide measured velocity field. Some regional-scale studies have been conducted (cf. Roer 2005), but most investigations are still concentrated on single rock glaciers and mesoscale information on this topic is limited. Area-wide data about the flow behaviour of rock glaciers provide useful input data for modelling rock glacier dynamics. From the calculated multi-temporal displacement rates conclusions can be drawn on driving factors of rock glacier creep.

Horizontal displacements of the investigated rock glaciers could be calculated from multitemporal aerial images and ALS data. Comparison between the surface displacement rasters and dGPS data indicate an accuracy (standard deviation) of the calculated displacement rates of 0.3 m for the period 2009 / 2010 respectively 0.5 m (0.13 for an annual scale) for the period 2006 / 2010. As AHK is a very fast creeping rock glacier, the data and method used is sufficient to receive significant results for almost all parts of the rock glacier. However, a time span smaller five years between the ALS data acquisition data and raster resolution of 0.5 m might not be long enough to obtain significant results for slow creeping rock glaciers.

The developed workflow could be easy adapted to the new ALS data from the area of Montafon (Vorarlberg) and the derivation of surface changes, which have been done on these single rock glaciers could be applied for the whole region to detect area wide surface changes. The Figures 3, 4 and 5 show results, which are derived from the orthoimages and ALS flight campaigns 2006 and 2009. They demonstrate the horizontal flow velocities between different periods. Table 6 shows the computed flow velocities from the orthoimages of AHK and RK.

In the case of AHK, permafrost creep is the most important factor governing local surface elevation changes. Future applications of ALS in rock glacier monitoring should focus on (I) the method's capability to quantify very slow creeping permafrost, (II) the performance on rock glaciers with small changes of local surface topography (smooth surface), (III) on the calculation of 3D displacements, and (IV) and area-wide quantification of rock glacier creep.

In the case of RK and AHK permafrost creep is the most important factor governing surface elevation changes. Computer-based aerial photogrammetry in combination with ALS allows detailed determination and analysis of surface elevation changes in and horizontal displacements on the investigated rock glaciers over a period of 56 years. These calculations build an important analytical component for identifying the state of activity of rock glaciers.

Using ALS data in rock glacier research, especially for validating the photogrammetrical derived DEMs, and for calculating flow velocities has proven to be a useful

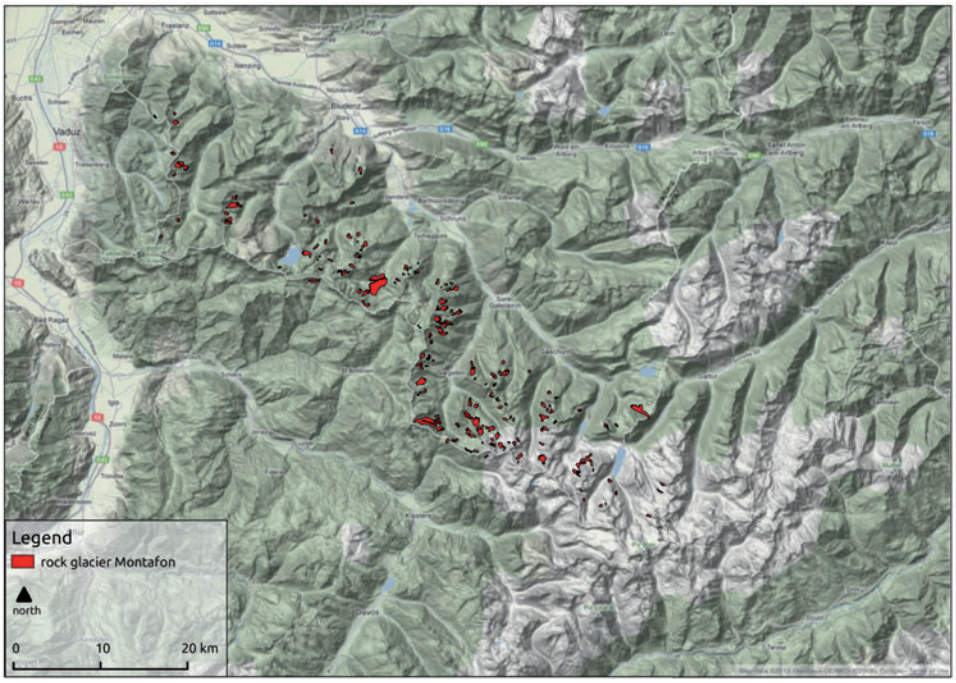

Figure 13: The Montafon range with the mapped rock glacier inventory

data source for area-wide investigations on rock glaciers. The results show the potential of the method combination to quantify spatio-temporal variations of rock glacier surface changes.

4.2 Rock glacier inventory of the Montafon based on ALS data

4.2.1 Data

As mentioned in section 3, the ALS campaign of the Montafon Range was organized by the Institute of Geography in the framework of the permAfrost project in autumn 2010. Due to bad weather conditions (snow fall in higher regions) the entire area could only be finished after a second campaign in autumn 2011. The missing ALS data of the Montafon Range have been delivered in autumn 2012. Figure 2 gives an overview of the measured flight trajectories in the Montafon Range. The ALS data were preprocessed by the responsible companies, which includes the determination of the absolute position and orientation of the laser scanning system during the flight, as well as the system calibration and strip adjustments (cf. Wehr & Lohr 1999). After preprocessing, the delivered last pulse ALS point clouds consisting of x, y and z coordinates were imported and stored in our laser data information system. Compared to the point density of the first flight campaign in 2010, the laser scanning data has been ordered with a point density of at least 4 pts / per m² (cf. Table 2).

ALS data quality control, data processing and its management process is analogue to that described in section 3. On the base of 72 measured dGPS points an average slope dependent vertical accuracy of approximately 14–35 cm could be calculated.

4.2.2 Method

The rock glacier inventory of the Montafon area was established based on field work, geomorphological maps and ortho-images. For the compilation of the inventory, we identified and delineated rock glaciers based on their specific morphological appearance (Barsch 1996) using colour orthophotos and laser scan images. Following Krainer & Ribis (2012), most rock glaciers could be easily recognized due to their typical morphological features. However, the definition of the upper boundary in the rooting zone was difficult and to some extent arbitrary. A few rock glaciers were difficult to recognize at all as their morphological outlines are not clearly defined. In these cases the surface morphology (indication downslope creep) was the criterion for definition as rock glacier. As a transition exist between large solifluction lobes and small rock glaciers, the size of a rock glaciers was defined by a minimum length of 50 m and a minimum width of 35 m. Altogether 193 rock glaciers were detected.

As rock glaciers have a highly complex surface topography, and furthermore the quality of our analysis strongly relies on an accurate terrain representation, we generated DTMs with 1 m x 1 m cell size for each rock glacier and its near surrounding (buffer of 200 m around the rock glacier outline). To do so, a mean function contained in SAGA GIS, was applied to generate a DTM of 2004 as well as of 2010 of each rock glacier. The mean function populates each grid cell with the average elevation values of all ALS points that are spatially contained within each cell. As the given point densities do not allow to populate each 1 m x 1 m DTM cell with elevation values directly, a close gaps tool was applied to populate cells that did not originally contain elevation values.

For the conduction of our study, we used the same rock glacier extents as derived in the compilation of the rock glacier inventory. Each rock glacier outline is defined by a polygon stored in shapefile. The usage of multi-temporal ALS datasets allowed the identification of terrain surface changes. Geometric changes of rock glaciers caused by melt, creep or material input are quantified by means of DTM differencing. For that purpose, thickness change $dDTM^n$ is calculated for each of the 193 rock glaciers (n = 1–193) by subtracting the 2004 DTM from the 2010 DTM with

$$dDTM^n = DTM^n - DTM^n \quad (2)$$

where $dDTM^n$ is the thickness change model of rock glacier n between 2004 and 2010, furthermore the area-averaged thickness change of each rock glacier was calculated. A first classification of the rock glaciers was done on the base of these ALS differences between 2004 and 2010.

4.2.3 Results and interpretation

In our study we assumed, that rock glacier thinning is caused by melt of internal ice followed by surface subsidence. Thus, thinning can only occur at intact rock glaciers. Regarding the spatial distribution and magnitude of thickness change on a whole rock glacier, the magnitude of thinning taking place in one part of the rock glacier might be balanced by frost heave or debris input in another part of the rock glacier. This would result in an area-averaged thickness change ($\overline{\Delta z^n}$) of 0 m leading to the erroneous conclusion that the rock glacier has to be relict. To overcome this problem of misinterpretation, the standard deviation σz^n was calculated, because it contains additional information about the spatial variability of the rock glacier deformation.

A large σz^n is considered to be representative either for an inactive rock glacier where different magnituds of thickness change occur at different areas on the rock glacier or for an active rock glacier where big σz^n is caused by the displacement of individual furrows and ridges of the rock glacier. In any case, rock glacier with big σz^n are considered to be more active than those with lower σz^n.

Figure 13 shows the map of the Montafon range with the distribution of all rock glaciers we kept into the inventory. The red colored polygons describe the shape of identified rock glaciers. The inventory could be filed up with the knowledge about the activities of each rock glacier. Based on the method described above, the rock glaciers were classified into inactive and intact. In the investigation area, there are only a few intact rock glaciers left.

Altogether 193 rock glaciers were detected. From these ten rock glaciers were classified as intact, and 173 as relict. Another ten rock glaciers could not be classified, as

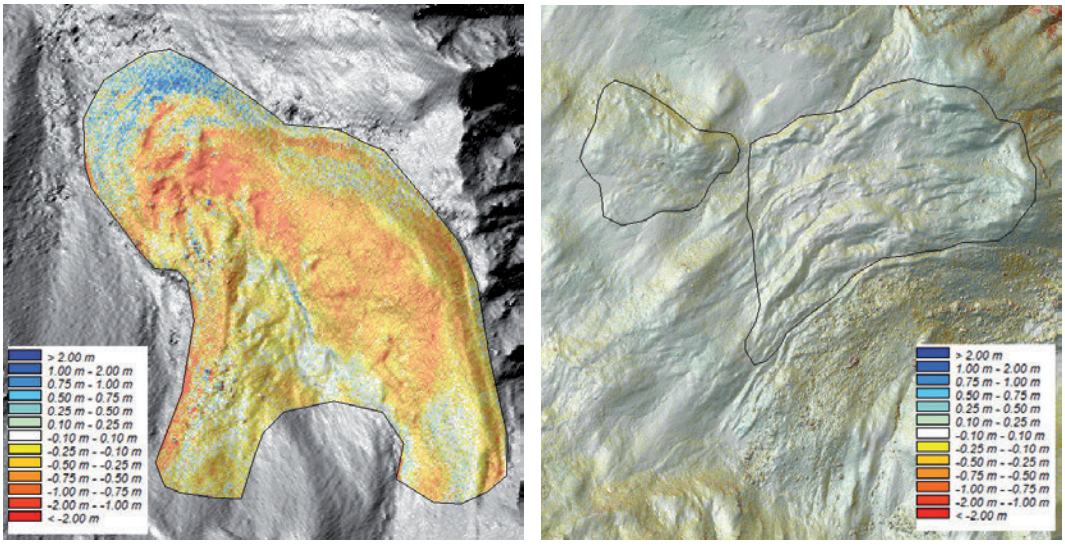

Figure 14: Two examples from the rock glacier inventory of the Montafon Range. (left) intact rock glacier; (right) two relict rock glaciers

they lie out of the area covered by the ALS data set. It was not as easy to distinguish intact rock glaciers seriously between active and inactive without knowledge about the movement rates, as this is the main criterion for a rock glacier being active or inactive (Barsch 1996).

Figure 14 shows two examples of the inventory with their elevation changes from 2004 to 2010. The right image shows an intact rock glacier with an area-averaged surface change of –0.38 m and a σz^n of about 0.41 m. The positive values along the rock glacier front are a visible sign for the movement of that permafrost body. The left image is an example of two relict rock glaciers with nearly no altitudinal changes ($\overline{\Delta z^n}$ = –0.03 m and σz^n = 0.02 m).

With the resulting rock glacier inventory, it will be possible to model the overall permafrost distribution in that region. Furthermore it is planned to calculate the horizontal displacement rates of the mapped intact rock glaciers in order to distinguish between inactive or active type.

Combining this dataset with the other existing inventories of Austria (e. g. Tyrol) and using the high resolution multi-temporal ALS data, an accurate large scale permafrost distribution model can be realized. These efforts are planned for subsequent project activities.

4.3 Detecting permafrost evidence on Rofenberg

4.3.1 Data and remote sensing approach

As mentioned in section 2 a test site was installed at the Rofenberg in the Ötztal Alps (Tyrol, Austria) to verify the remote sensing based insights about permafrost induced surface changes. Since 2001, ALS measurements have been carried out regularly at Hintereisferner and the adjacent Rofenberg, resulting in a unique data record of 21 ALS flight campaigns until now. A summary of the available ALS campaigns, and their corresponding system parameters, is given in Sailer et al. (2012). Regarding the accuracy of the ALS data series, Bollmann et al. (2011) indicate an absolute vertical accuracy of 0.07 m with a standard deviation of ± 0.08 m. The results are based on a comparison of dGPS points with the nearest neighbouring ALS points on the relatively flat and smooth glacier tongue of Hintereisferner.

As the experimental design (sensor types, height above ground, geo-referencing and transformation parameters) of all ALS campaigns were nearly uniform, the slope dependent error is very small (± 0.05 m for slope angles < 40°), compared to previously reported values. The delineation of possible permafrost areas, which are characterised by process induced surface altitudinal changes, was based on visual inspections of annual and multi-annual dDTM (differential DTM). In near proximity to the detected areas, stable areas, where no altitudinal changes were observed, are defined. These stable areas are used for i) quantitative correction of the process related altitudinal changes or ii) to discard a specific dataset if necessary (cf. Fig. 15; cf. Sailer et al. 2012).

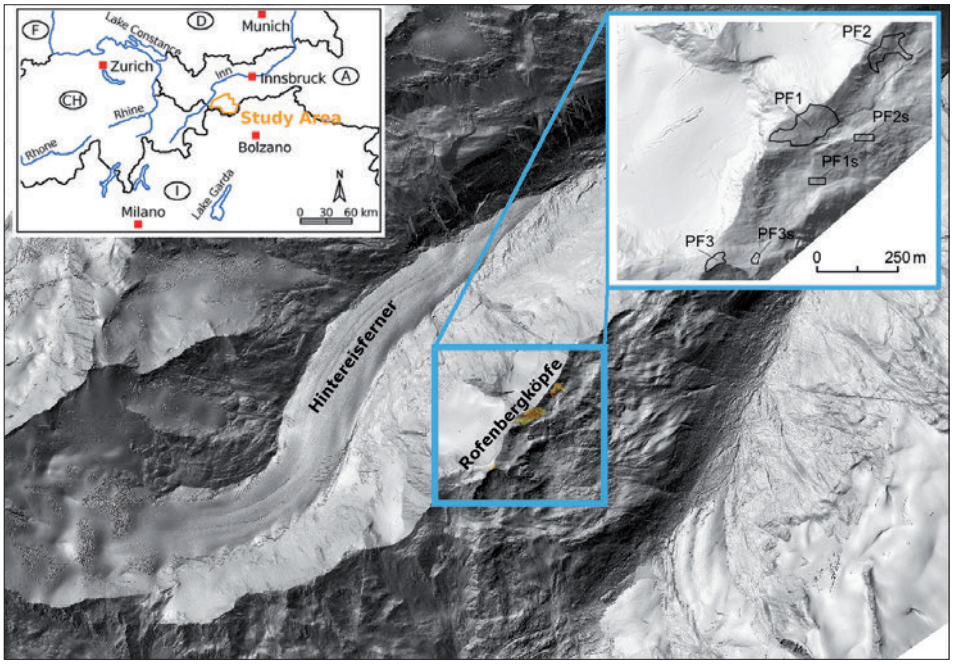

Figure 15: Location of the study area and the exemplary areas of surface lowering (PF I–III). (Cartographic basemap: ALS DTM, Institute of Geography, Innsbruck 2011)

At several small areas near the mountain ridge of the "Rofenbergköpfe" south of the glacier tongue of Hintereisferner, a small but continuous lowering of the surface (cf. Table 7) was detected throughout the whole data series of 22 ALS flights. Those surface changes were assumed to originate from the melting of permafrost or small dead-ice bodies. To verify this assumption, several measurements have been done or prepared.

Table 7: Annual altitudinal changes dz (m) to the reference level 2011 of possible permafrost and stable areas (cf. point-based results in Sailer et al. 2012 and accuracy assessment in Sailer et al. 2013)

			2010	2009	2008	2007	2006	2005	2004	2003	2002	2001
permafrost areas	PF1	dz process	–0.06	0.04	–0.09	–0.33	–0.39	–0.64	–0.36	–0.42	–0.48	–0.96
		dz stable (PF1s)	0.10	0.10	0.10	–0.07	–0.19	–0.45	–0.06	–0.06	–0.15	–0.36
		dz process corrected	–0.16	–0.06	–0.19	–0.26	–0.20	–0.19	–0.30	–0.36	–0.33	–0.60
	PF2	dz process	–0.01	–0.04	–0.03	–0.29	–0.29	–0.69	–0.29	–0.35	–0.40	–0.97
		dz stable (PF2s)	0.11	0.10	0.11	–0.18	–0.18	–0.52	–0.09	–0.02	–0.14	–0.37
		dz process corrected	–0.12	–0.14	–0.14	–0.12	–0.11	–0.17	–0.20	–0.33	–0.26	–0.60
	PF3	dz process	–0.21	–0.21	–0.05	–0.38	–0.32	–0.70	–0.33	–0.29	–0.40	–0.95
		dz stable (PF3s)	–0.06	0.03	0.10	–0.26	–0.17	–0.80	–0.14	0.00	–0.11	–0.42
		dz process corrected	–0.15	–0.24	–0.15	–0.12	–0.15	0.10	–0.19	–0.29	–0.29	–0.53

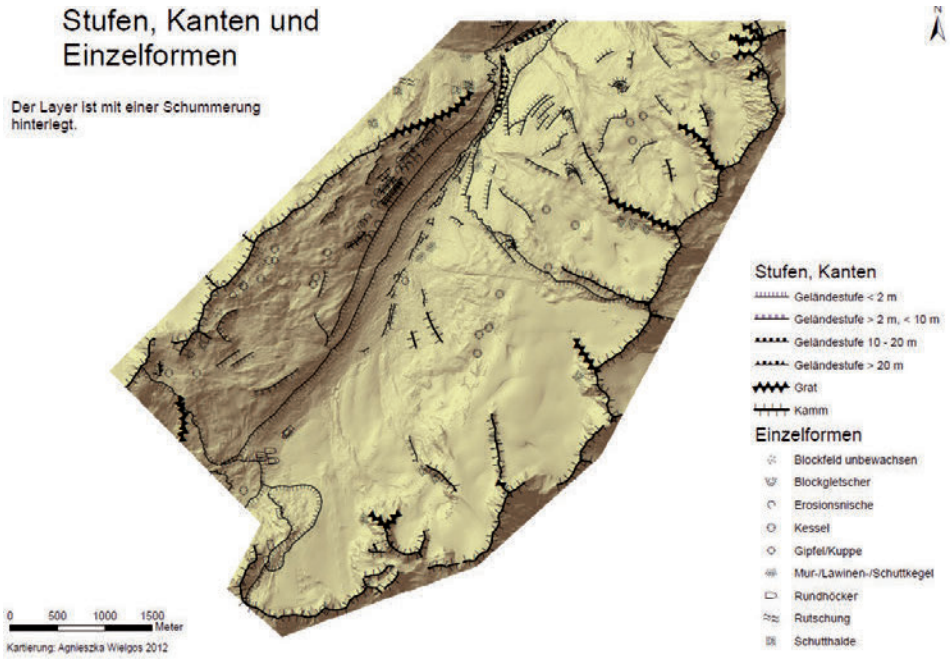

Figure 16: Geomorphological map of Rofenberg

Figure 18 shows the local distribution of the different measurements. The annual surface elevation changes in the detected permafrost areas are very low (between –0.05 m and –0.10 m per year). Therefore, the significance of the process dependant measured topographic change rates was assessed with special regard to the accuracy of the ALS data, the magnitude of the process, the time lapse between the single ALS-campaigns and frequency and disturbing factors (e. g. snow cover). Results gained in significance with increasing time laps between the ALS-campaigns, the frequency of flight campaigns and if disturbing factors (e. g. snow cover) can be excluded.

4.3.2 Methods

4.3.2.1 Geomorphologic mapping

In the course of geomorphologic mapping on Rofenberg different approaches have been applied. Firstly, intensive field investigations have been conducted. In a second step, the mapped surface structures have been cross checked with a geoinformatic approach. Therefore the ALS data have been processed with an automatic breakline detection tool implemented in GRASS GIS (Rutzinger et al. 2010). To get clear results the mapped and automatic derived surface structures have been adjusted using an orthoimage and a shaded relief (acquisition time September 2010) and a difference layer of the DTMs of 2006 and 2010. The geomorphological mapping has

been conducted using a legend for high mountain geomorphology, which is based on GMK 25 (cf. Kneisel et al. 1998; Fig. 16).

4.3.2.2 BTS measurements and BTS loggers

Measurements of ground temperatures of the winter snow cover (the so called BTS method) are a well-established technique to map mountain permafrost. Hereby, a probe is pushed through the snow cover to the ground surface. An important boundary condition for the successful application of this method is a sufficiently thick (at least 60–80 cm) snow cover. The snow cover, with its low thermal conductivity, insulates the ground from short-term fluctuations in air temperature. If the winter snow

Table 8: Coordinates and terrain description of the 15 temperature loggers displaced on Rofenberg

	UTM-Coordinates	Z [m a. s. l]	Description of area around logger
1	637163 E, 5184507 N	3,033	flat crest, stone diameter: 2–20 cm Soil and fine-grained substrate
2	637123 E, 5184101 N	3,041	flat area, flat crest, fine-grained material (gravel / sand), stone diameter 5–20 cm (10% > 20 cm), no local shading, shallow weathered layer on top of bedrock (ca. 0.5 m)
3	637057 E, 5184143 N	3,048	logger underneath small boulder (diameter 50 cm), east-facing, flat, small crest surrounded by surface water, stones 10–20 cm, no local shading, snow rich area
4	636963 E, 5184175 N	3,070	logger hanging on a lash (40 cm long) in blocky area, always in shade, no fine-grained material, boulder: 0.5–1 m, crest, rock fall material
5	636310 E, 5184489 N	3,203	boulder material d = 60 cm, no fine-grained material, SE, 23°
6	636876 E, 5184543 N	3,213	SE, 25°, boulder with d = 40 cm
7	636950 E, 5184586 N	3,173	East, 35°, boulder with d = 50 cm
8	637030 E, 5184582 N	3,164	blocky material d = 60 cm, individual ”moss pillows“, east, flat area, 5°
9	637058 E, 5184592 N	3,144	flat, depression with d = 30 m, sand / gravel, stones d = 20 cm
10	637088 E, 5184688 N	3,132	small basin with d = 20 m, depression, snow rich, flat, no topographic shading
11	637146 E, 5184743 N	3,125	flat, crest, no topographic shading, stones with d = 20 cm, some fine-grained material, sporadic moss/grass
12	637066 E, 5184779 N	3,156	SEE, 18°, „flat area“ with 80 m x 30 m, frost affected surface, sandy, stones < 10 cm individual with 30 cm, distance to main crest ca. 20 m horizontal
13	637167 E, 5184777 N	3,112	depression, snow rich, logger hanging on a lash 10 cm underneath surface, blocky, depression NE facing, 25°
14	637517 E, 5184863 N	3,016	same exposition as logger 15 (SO), depression (below crest 50 vertical m, 150 horizontal m), fine-grained material available, logger on “soil“ but covered with flat stone, stone diameter < 40 cm
15	637707 E, 5184684 N	2,941	flat area, grass, fine-grained material (sand, gravel), few stones, micro exposition South,

Figure 17: BTS measurements on Rofenberg, March 2011, photograph by L. Rieg

cover is sufficiently thick and surface melting is still negligible in mid- to late winter, the BTS values remain nearly constant and are mainly controlled by the heat transfer from the upper ground layers, which in turn is strongly influenced by the presence or absence of permafrost. Values obtained over permafrost are below –3 °C. Values between –2 and –3 °C represent the uncertainty range of the method and/or marginally active permafrost with thick active layer, which does not totally refreeze during winter. At permafrost-free sites or sites with inactive permafrost the measured values are above –2 °C (Haeberli 1996).

In addition to spot measurements of the BTS, 15 temperature loggers (see Table 8) were placed to record the BTS and year-round near-surface temperatures. From the latter data the mean annual ground surface temperature (MAGST) can be calculated. According to van Everdingen (1998), permafrost exists if the MAGST is perennially below 0 °C. Concerning the MAGST, the thermal offset, which is defined as the difference between mean annual temperature at the permafrost table and the mean annual ground surface temperature, has to be taken into account. Burn and Smith (1988) have suggested that permafrost may be in equilibrium, or aggrading, even under conditions where the mean annual ground surface temperature is slightly above 0 °C.

Figure 18: Temperature logger distribution. Observation point 14 located at Rofenberg at 3,000 m a. s. l., photograph by E. Bollmann

In spring 2011 (30.03.2011) and 2012 (2.04.2012) the base

temperature of the snow pack (BTS) was measured in the whole area close to the end of the winter snow accumulation period, to get a general idea of the possible distribution of permafrost or ice in the underground. Five probes were placed in a circular arrangement as it is shown in Figure 17. The data were collected between altitudes above and beneath the lower boundary of discontinuous permafrost.

For further investigations on the occurrence and distribution of permafrost, 15 BTS loggers were installed in order to measure the temperature during the winter. This allows recording the potential freezing and thawing of the underlying soil. The loggers are distributed over different elevation levels to detect the lower boundary of discontinuous permafrost (Fig. 18 and Table 8).

4.3.2.3 Geophysical surveys

Geophysical methods are particularly suitable for geomorphological investigations, since the knowledge of structure, layering and composition of the subsurface at different scales are key parameters for geomorphological problems. Georadar, geoelectric and seismic methods were used to detect permafrost, with each geophysical method being applied on all profile lines. This parallel application enabled us to compare and cross-validate the results of the three techniques. After the analyses of the single datasets, a tomography including all results was created.

In July and September 2011, geophysical measurements were carried out at two selected sites on Rofenberg (Fig. 19). Three profiles (B, C, D) were measured at a height of about 3,200 m. Two of them were parallel and one was crossing them both.

Figure 19: Geophysical field measurements on Rofenberg, July 2011, photograph by C. Klug

Each profile had a length of about 100 m. The spacing of the electrodes was 2 m for geoelectrical measurements using Wenner geometries. The geophone spacing for seismic measurements was about 4 m and a shot spacing of 4 m was applied. For georadar measurements 50 MHz, 100 MHz and 200 MHz antennas were used. Moreover, another profile (A) was measured at a height of around 2,900 m a. s. l. with nearly the same calibrations (cf. Fig. 20).

4.3.3 Results and Interpretation

The occurrence of settlement features that might be related to melting permafrost provides a first geomorphological evidence of permafrost occurrence. This verifies the assumption that the small but continuous lowering of the surface (cf. Table 7), which was detected throughout the whole data series of 22 ALS flights, originates from the melting of permafrost.

According to BTS measurements, performed in spring 2011 and 2012, the higher parts of the investigated area between 3,200 and 3,300 m a. s. l., are underlain by permafrost. Measurements were recorded that are mostly below –3 °C, moreover at three measurements are at least within the uncertainty range of the method (–2 to –3 °C). In the lower parts of Rofenberg, permafrost is mapped as improbable (Fig. 20).

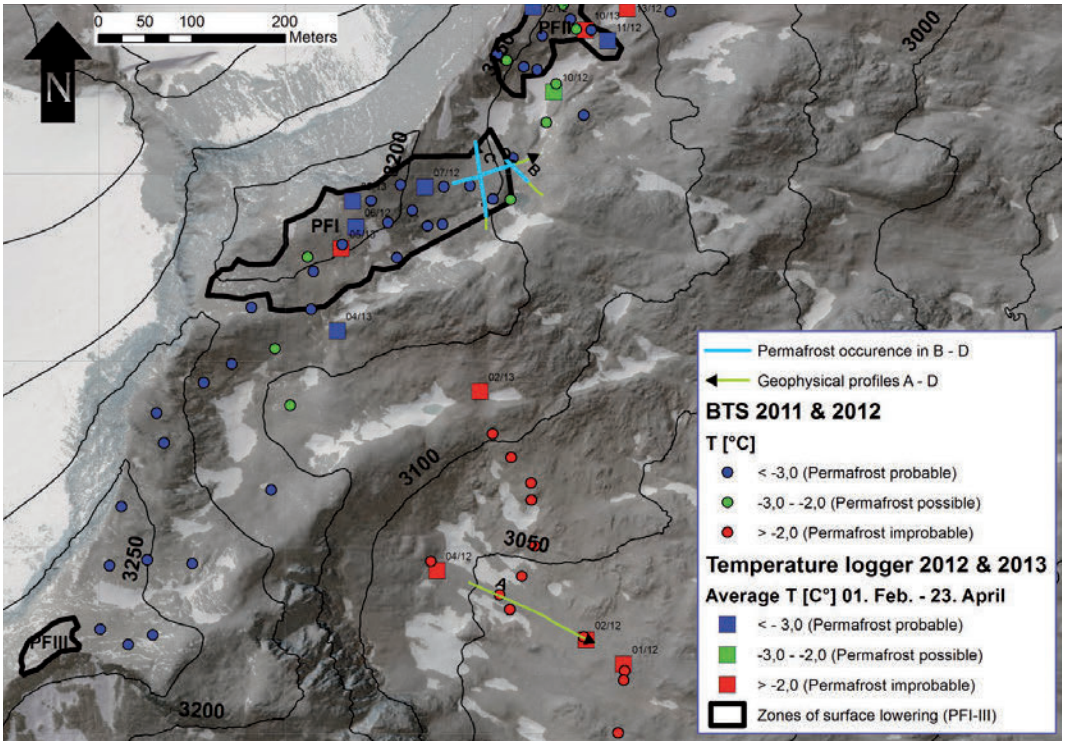

Figure 20: BTS measurements and GST lgging on Rofenberg

These results are supported by findings from the geophysical measurements and measured year-round near-surface ground temperatures for the period September 2011 until September 2012, which were recorded using fifteen miniature loggers.

In order to assess ground thermal conditions, the temperature loggers were placed in the upper parts of the supposed permafrost areas and near the geophysical profiles. Twelve of the 15 loggers were obviously covered by a thick enough snow cover, as there are no high frequency variations visible in the graph and the values decrease gradually until the final more or less constant temperature is reached in the mid to late winter months. Thus, the bottom temperatures of the snow cover can be analysed according to the three distinguished BTS classes. From the beginning of May an increase of the temperatures to 0 °C is visible; in the following weeks the temperatures remain constant around 0 °C (zero curtain). This feature is typical for mountain permafrost with dry freezing in autumn without development of a zero curtain and wet thawing in spring with pronounced zero curtain (cf. Kneisel & Kääb 2007).

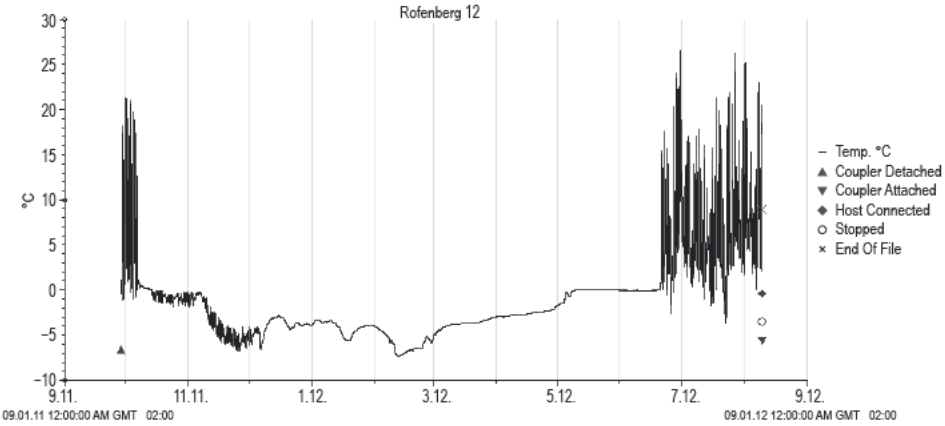

Figure 21: Result of BTS-logger (no. 12) on Rofenberg. Recording time: 27.09.2011–12.09.2012

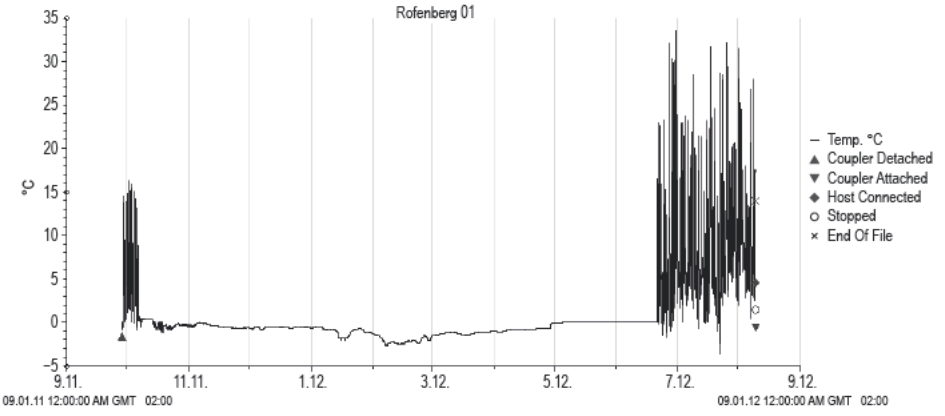

Figure 22: Result of BTS-logger (no. 1) on Rofenberg. Recording time: 27.09.2011–12.09.2012

In the winter period the loggers 6 to 12 recorded BTS values that indicate permafrost. Mean annual ground surface temperatures could be calculated for the period 27 September 2011 to 12 September 2012. The results with negative mean annual ground temperatures (e. g. logger 12: –1.43 °C) point to permafrost favourable conditions during the measurement period. The survey presented in Figure 21 was performed on the uppermost part of Rofenberg, where BTS measurements point to the presence of permafrost (Fig. 20). In contrast the logger 1 (Fig. 22), situated in the lowest part of Rofenberg, shows positive MAGST, which is in good accordance with the BTS measurements there and indicates that permafrost is improbable.

4.3.3.1 Ground Penetrating Radar (GPR) results

GPR results for the upper three profiles (cf. Fig. 23, 24 and 25) show reflectors close to the surface that are all present for the most part of the profiles. Deeper regions of the profiles show continuous reflectors in a depth of about 10 and 22 m for profile D (Fig. 23) and profile B (Fig. 25). Profile C shows a close to the surface reflector that follows the whole profile as well (Fig. 24). Deeper regions in this profile cannot be interpreted by using radar due to low signal to noise ratio. Similar depths of reflectors for those three profiles are consequentially because all profiles are based in the same area. Profile A (Fig. 26) being based several hundred meters away shows reflectors in a depth of about three and nine meters, but they are less significant than in the upper zone.

4.3.3.2 Electric Resistivity Tomography (ERT) results

The ERT results for all profiles show resistivities later being interpreted as permafrost. Table 9 gives the specific resistivities of relevant materials. Especially profile C (Fig. 27) and B (Fig. 28) fit together well. You can see a low resistivity zone (ca.

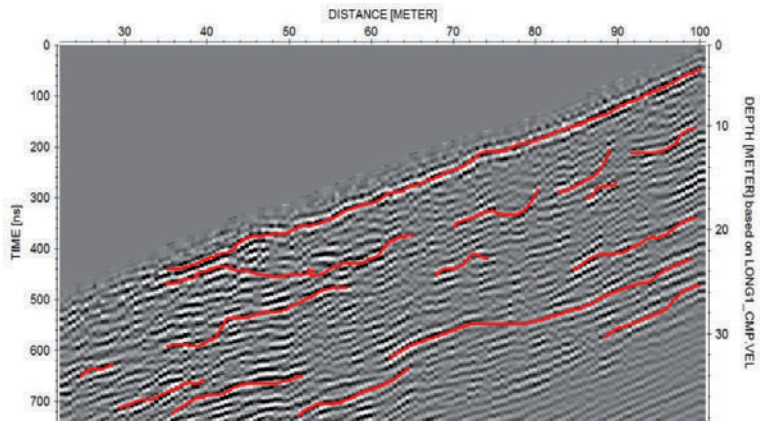

Figure 23: Profile D measured with 50 MHz. Reflector 1 proceeds close to the surface in a depth of about 2 m. Reflector 2 starts at a depth of 2 m, descending until 10 m depth after short distance being visible until the end of the profile. Deeper regions show further reflectors in a depth of about 22 m.

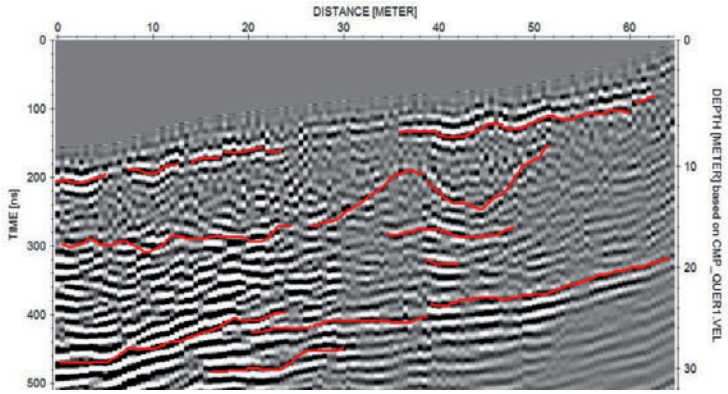

Figure 24: Profile B measured with 50 MHz. This profile shows quite similar results as profile D. Reflector 1 proceeds in a depth of about 2 to 3 m and is visible until the end of the profile. Another reflector is visible in a depth of about 10 m. The reflections in about 22 m depth are visible in this profile as well

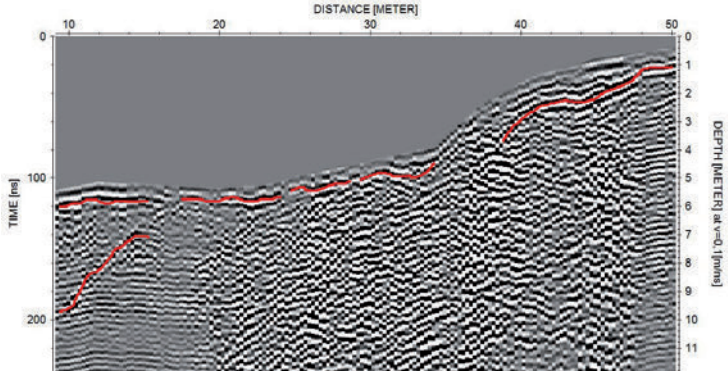

Figure 25: Profile C measured with 200 MHz. This profile shows one reflector close to the surface in a depth of about 2 m. Further reflectors in deeper regions can't be interpreted due to low signal to noise ratio

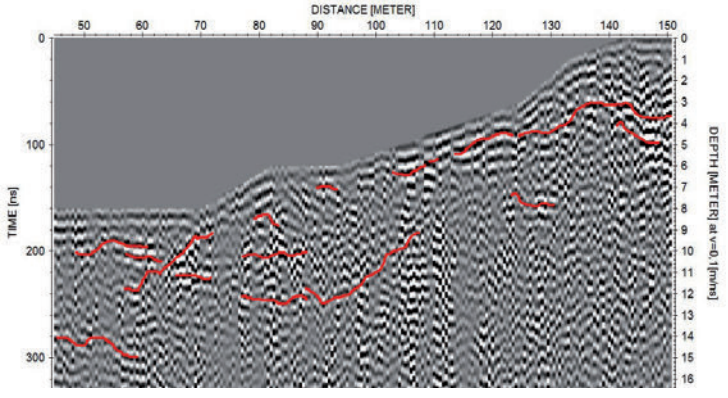

Figure 26: Profile A measured with 100 MHz. One reflector in a depth of about 2 m can be seen in this profile. Another reflector is interpreted in a depth of about 8 m

1,500 Ωm) starting at 32 m x-distance up to 3 m depth which fit to sand and gravel of the surface. This area is followed by a zone up to 10 m depth with high resisitivities which fit well to permafrost. Profile B shows a high resistivity area starting from 28 m x-distance up to a depth of 10 m. This also fits to permafrost. The low resistivity zone (ca. 700 Ωm) at the beginning of profile B is related to a small lake to the profile so this area is saturated with water. In profile A no significant resistivity zone concerning the permafrost was found.

Table 9: Specific resistivities of relevant materials (Knödel et al. 1997; Maurer & Hauck 2007)

Materials	Range of resistivity [Ωm]
Air	infinite
(Ground-) Water	10–300
Sand/Gravel	100–10^4
Metamorphic rock	1 000–10^5
Permafrost	5 000–10^6
Glacial ice	10^5–10^7

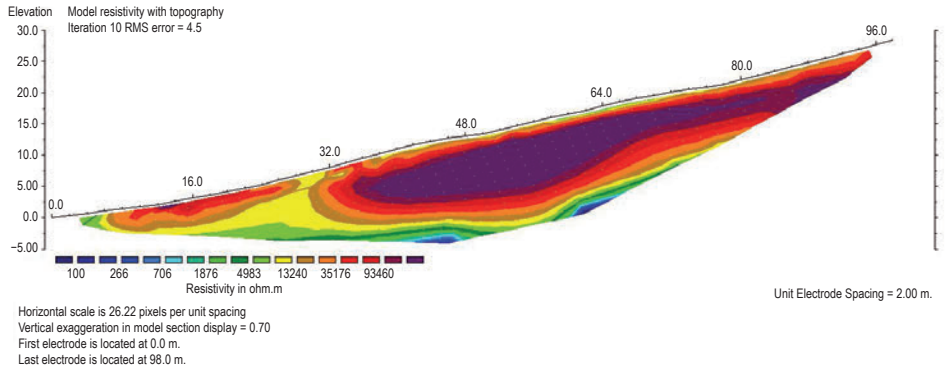

Figure 27: ERT of profile D. You can see two purple areas with high resistivities. The first area up to 28 m x-distance fit to the ice rich gravel on the ground. The area starting at 32 m x-distance is interpreted as permafrost. The upper 2 m have lower resistivities fitting to the surface gravel

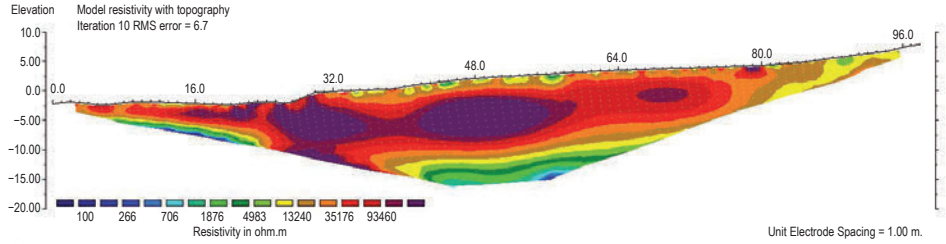

Figure 28: ERT of profile C. The purple red area starting at 32 m x-distance fits to permafrost. The area from zero to 32 m x-distance was covered by snow and there was a dyke between 20 m and 32 m filled with snow, therefore in this area you can see big resisitivities. Up to 3 m depth starting at 32 m x-distance the resisitvities fit to the surface gravel

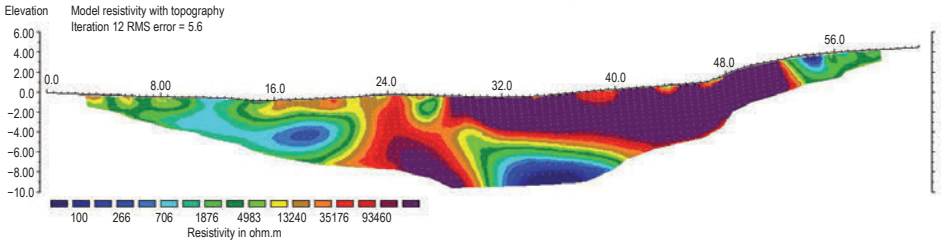

Figure 29: ERT of Profile B. Here you can see a blue are between 8 to 20 m x-distance which is related to a sea near to the profile and therefore the underground is saturated with water. The big purple area starting at 30 m x-distance fits to permafrost

4.3.3.3 Seismic Refraction Tomography (SRT) results

It was only possible to measure the SRT at profile D and 70% of profile C due to technical problems. Both profiles show slow seismic velocities up to a depth of 2 to 3 m (Fig. 30 and 31; ca. 1,000 m/s) followed by an area of velocities between 2,500 and 3,500 m/s (cf. Table 10). The first area represents the surface with sand and gravel and the deeper area fits to the velocity range of Permafrost. In Figure 30 you can also spot a zone with velocities up to 5,000 m/s which fits to metamorphic rock and could represent the bedrock.

For evaluating an underground model of the measured area all three methods

Table 10: Seismic velocities for relevant materials (Hecht 2001; Knödel et al. 1997; Maurer & Hauck 2007)

Material	Seismic Velocity (m/s)
Air	330
Water	1,400–1,600
Sand/Gravel	300–2,000
Boulder	600–2,500
Morainal material / Glacial sediments	1,500–2,700
Metamorphic rock	3,000–5,700
Permafrost	2,400–4,300
Glacial ice	3,100–4,500

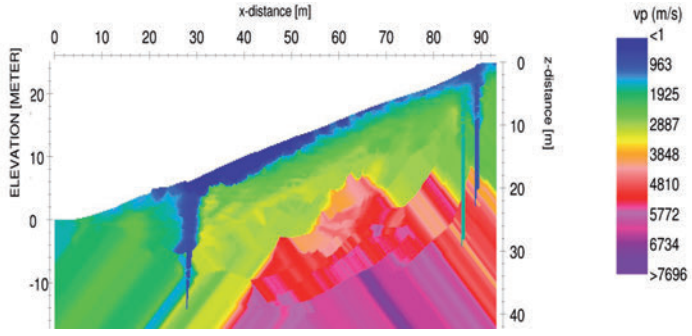

Figure 30: SRT Velocity model of Profile D. You can see the sand/gravel area (blue) up to 3 m depth. The green/yellow area starting at 25 m x-distance fits to Permafrost. Up to 25 m x-distance in depths up to 3 m the velocities are higher than in the other surface areas due to visible ice rich gravel. In depths starting at 15 m depth the red area fits to metamorphic rock with velocities up to 5,000 m/s

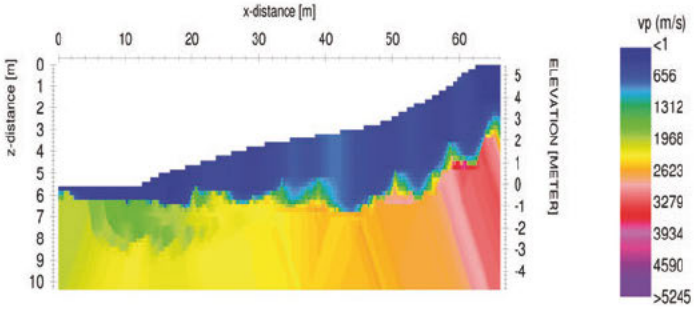

Figure 31: SRT Velocity model of Profile B. You can spot the blue area of gravel like velocities in depths up to 3 m following by an area (yellow/orange) which fits to permafrost with velocities over 2,300 m/s. Due to technical problems it was only possible to measure 70% of this profile. 65 m x-distance is equivalent to 96 m x-distance of the ERT

were combined by overlaying the results. The finished models are shown in Figure 32–34. Permafrost was interpreted in all four profiles.

Figure 32 shows the model of profile D where you can see a permafrost layer with 64 m length and up to 10 m depth. The permafrost layer of profile B (Fig. 33) has

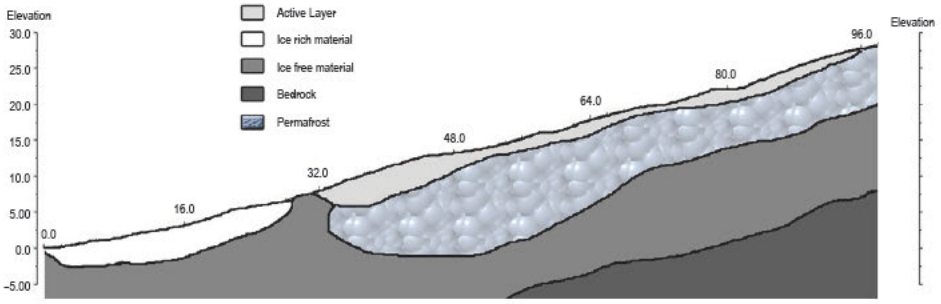

Figure 32: Underground model of profile D. The active layer could be sawn clearly and permafrost is also interpreted. Furthermore the ice rich surface was represented in the data

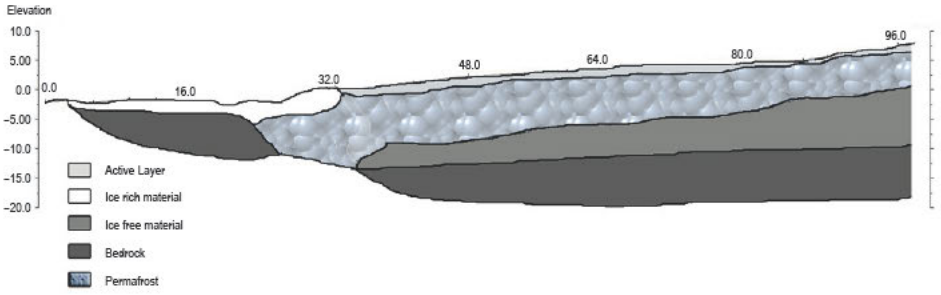

Figure 33: Underground model of Profile B. The snow dyke is detected in the data and also a permafrost body could be interpreted as well as the active layer

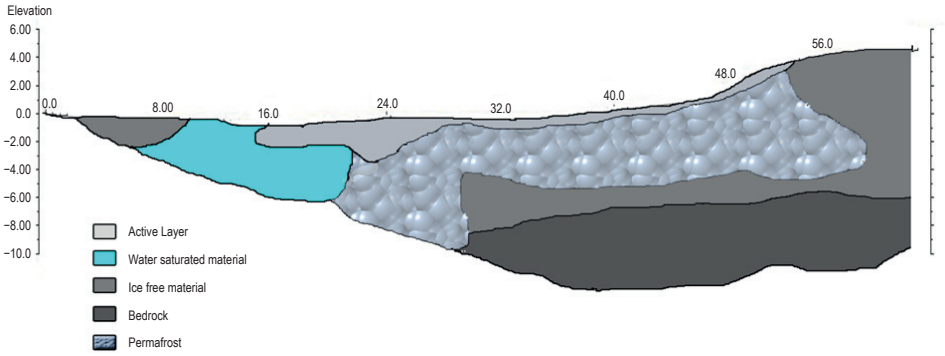

Figure 34: Underground model of profile D. A clear permafrost layer could be interpreted. The active layer is also represented in the data as well as a water saturated area as result of the sea near the profile

a length of 75 m and a mean depth of 5 m. In Figure 34 you see the model of profile C with a permafrost layer of about 34 m length and 2–6 m depth. In the area of profile A no permafrost was detected. The proportions are about a length of 60 m and a depth of 13 m.

5 Overall Conclusions

Several geomorphologic changes due to melting permafrost were detected including the occurrence of rock glaciers. The studies of Sailer et al. (2012), which are related to the project permAfrost, provide detailed investigations of the quantification of geomorphodynamics. Surface elevation changes or single rock fall events, which may be caused by thawing permafrost, were detected with the help of multi-temporal ALS data.

All presented methods and workflows have to be applied in combination in order to provide an operational methodology for on-going, spatially continuous and area-wide monitoring of geomorphological significant permafrost change. Especially multi-temporal ALS is useful for the large scale investigations. As a second step, the findings of that remote sensing based approach have to be verified with in-situ investigations like BTS and / or geophysical measurements (e. g. ERT). The results we described above demonstrate the capability detecting permafrost spatially continuous and area-wide. However, successful investigations depend strongly on the data quality (e. g. ALS). Even financial efforts, especially when acquiring ALS flight campaigns, may not be underestimated, as this technology is still very cost-intensive.

Geomorphological observations, ALS based remote sensing approaches, BTS measurements and geophysical measurements on the Rofenberg were used to obtain an integrative analysis of a highly complex periglacial landform. A valuable aspect of modern geophysical techniques and their application in geomorphology is the ability to image the subsurface.

Table 11: Overview of the applied methods

Method	Pros and cons	Ability	Requirements
ALS	+ • Provides operational tool for spatially continuous and area-wide monitoring of permafrost (PF) change • High resolution (0.5 m) possible • High vertical accuracy • Operational stage • Contact free – Cost intensive Weather condition dependent	• High vertical accuracy allows detection of PF degradation • Possibility of individual flight planning (research area, resolution, acquisition date)	• Flyable weather • High temporal resolution (annual, inter-annual, decadal) for different processes • Data storage, management and processing tools • Sufficient point density
Aerial images	+ • Provides an operational tool for spatially continuous and area-wide monitoring of PF change • Long-time monitoring (back to 1950s) • High horizontal accuracy • Operational stage • Combinable with ALS • Contact free – • Less cost intensive • Shadowing and bad contrast effects • Lower vertical accuracy and lower resolution than ALS	• Long-time monitoring (back to 1950s) • High horizontal accuracy allows mapping of morphological PF features	• Avoiding of shadowing and bad contrast effects • High temporal resolution (annual, decadal) for different processes • Overlapping images for DTM generation
Geophysics	+ • Tool for local monitoring of permafrost • Subsurface surveys – • Less information about surface changes • Not area-wide • Time consuming • Bulky instruments for field investigation	• Provision of subsurface information • Information of subsurface PF distribution • Ice content estimation of the ice body	• Combination of geophysical methods for better results • Accessibility • Expert know-how
BTS	+ • Tool for local monitoring of permafrost • Good significance on PF occurrence – • Time consuming • Not area-wide	• In situ evidence of PF presence • Verification of PF distribution models	• Snow conditions (> 60 cm snow cover) • Consistent spatial distribution of point measurements • Measurement at the end of accumulation period (BTS-probing)
Geomorphological mapping	+ • Good first basis for PF investigation • Less information about surface changes – • Time consuming • Subjectivity of the results	• Ability for first research questions • Detection of geomorphologic features to gain information about recent or past PF activities	• Combination of field investigations and remote sensing necessary

The agreement between the ALS based measurements and geophysical surveys presented on Rofenberg demonstrated that the investigation of surface changes by DTM differencing in cold mountain environments can be a suitable tool to detect surface deformation as a proxy for ice-containing permafrost. The combined approach allows a better understanding of the recent interplay between ice content and surface deformation. Hereby, integrative analyses have the potential to improve the understanding of permafrost-related periglacial landforms, which may exhibit active (supersaturated with ice and creeping), inactive (degrading ice and almost no creeping) and relict (ice-free, no creeping) sediment bodies in close proximity.

Concerning the main objectives, namely the detection of locations, where melting of permafrost leads to geomorphologic changes, and the provision of an operational methodology for on-going, spatially continuous, area-wide monitoring of geomorphological significant permafrost change, we tried out different methods. Table 11 gives an overview of the applied methods, their pros and cons and their ability in permafrost research and their requirements for good and interpretative results concerning permafrost degradation.

6 References

Barsch, D. 1996: *Rock glaciers. Indicators for the Present and Former Geoecology in High Mountain Environments.* Berlin.

Baltsavias, E. 1999: Airborne laser scanning: basic relations and formulas. *ISPRS Journal of photogrammetry and remote sensing* 54: 199–214.

Baltsavias, E.P., E. Favey, A. Bauder, H. Boesch & M. Pateraki 2001: Digital surface modelling by airborne laser scanning and digital photogrammetry for glacier monitoring. *Photogrammetric Record* 17, 98: 243–273.

Bauer, A., G. Paar & V. Kaufmann 2003: Terrestrial laser scanning for rock glacier monitoring. In: Phillips M., S.M. Springman & L.U. Arenson (eds.): *Permafrost: Proceedings of the 8th International Conference on Permafrost*, Zurich, Switzerland, 21-25 July 2003: 55–60.

Bollmann, E., R. Sailer, C. Briese, J. Stötter, & P. Fritzmann 2010: Potential of airborne laser scanning for geomorphologic feature and process detection and quantification in high alpine mountains. *Zeitschrift für Geomorphologie* 54 (Suppl. Issue 2): 83–104.

Bollmann, E., J. Abermann, C. Klug, R. Sailer & J. Stötter (2012): Quantifying Rock glacier Creep using Airborne Laserscanning. A case study from two Rock glaciers in the Austrian Alps. In: Hinkel, K.M. (ed.): *Proceedings of the Tenth International Conference on Permafrost*, Salekhard, Russia, 25-29 June 2012. Vol. 1: International Contributions: 49–54.

Dowdeswell, J.A. & T.J. Benham 2003: A surge of Perseibreen, Svalbard, examined using aerial photography and ASTER high resolution satellite imagery. *Polar research*, 22,2: 373–383.

Haeberli, W. 1982: Creep of mountain permafrost: Internal structure and flow of alpine rock glaciers. *Mitteilungen der Versuchsanstalt für Wasserbau, Hydrologie und Glaziologie ETH Zürich* 77: 1–142.

Haeberli, W. & G. Patzelt 1982: Permafrostkartierung im Gebiet der Hochebenkar-Blockgletscher. Obergurgl, Ötztaler Alpen. *Zeitschrift für Gletscherkunde und Glazialgeologie* 18, 2: 127–150.

Haeberli, W., B. Hallet, L. Arenson, R. Elconin, O. Humlum, A. Kääb, V. Kaufmann, B. Ladanyi, N. Matsuoka & D. Vonder Mühll 2006: Permafrost creep and rock glacier dynamics. P*ermafrost and periglacial processes* 17, 3, 189–214.

Hausmann, H., K. Krainer, E. Brückl & W. Mostler 2007: Internal Structure and Ice Content of Reichenkar Rock Glacier (Stubai Alps, Austria) Assessed by Geophysical Investigations. P*ermafrost and Periglacial Processes* 18: 351–367.

Hecht, S. 2001: *Anwendung refraktionsseismischer Methoden zur Erkundung des oberflächennahen Untergrundes.* Stuttgarter Geographische Studien, 131. Stuttgart.

Hodgsonn, M. & P. Bresnahan 2004: Accuracy of airborne Lidar-derived elevation: Empirical assessment and error budget. *Photogrammetric engineering and remote sensing* 70, 3: 331–339.

Hulbe, C.L., T.A. Scambos, T. Youngberg & A.K. Lamb 2008: Patterns of glacier response to disintegration of the Larsen B ice shelf, Antarctic Peninsula. *Global and planetary change* 63: 1–8.

Jackson, M., I.A. Brown & H. Elvehøy 2005: Velocity measurements on Engabreen, Norway. *Annals of glaciology* 42: 29–34.

Jokinen, O. & T. Geist 2010: Accuracy aspects in topographical change detection of glacier surface. In: Pellikka, P. & W.G. Rees (eds.): *Remote sensing of glaciers. Techniques for topographic, spatial and thematic mapping of glaciers.* London: 269–283.

Kääb, A. & M. Vollmer 2000: Surface geometry, thickness changes and flowfields on creeping mountain permafrost: automatic extraction by digital image analysis. *Permafrost and Periglacial Processes* 11, 4): 315–326.

Kääb, A. 2004: *Mountain glaciers and permafrost creep. Research perspectives from earth observation technologies and geoinformatics*. Habilitation. Department of Geography, ETH Zürich.

Kääb, A. 2010: Aerial photogrammetry in glacier studies. In: Pellikka, P. & W.G. Rees (eds.): *Remote Sensing of Glaciers. Techniques for Topographic, Spatial and Thematic Mapping of Glaciers.* London: 115-136.

Kääb, A., R. Frauenfelder & I. Roer 2007: On the reaction of rock glacier creep to surface temperature variations. *Global and planetary change* 56: 172–187.

Kääb, A., W. Haeberli & H. Gudmundsson 1997: Analysing the creep of mountain permafrost using high precision aerial photogrammetry: 25 years of monitoring Gruben rock glacier, Swiss Alps. *Permafrost and periglacial processes* 8: 409–426.

Kääb, A., V. Kaufmann, R. Ladstädter & T. Eiken 2003: Rock glacier dynamics: implications from high-resolution measurements of surface velocity fields. In: Phillips M., S.M. Springman & L.U. Arenson (eds.): *Permafrost: Proceedings of the 8th International Conference on Permafrost*, Zurich, Switzerland, 21-25 July 2003: 501–506.

Kääb, A., K. Isaksen, T. Eiken & H. Farbot 2002: Geometry and dynamics of two lobe-shaped rock glaciers in the permafrost of Svalbard. *Norsk geografisk tidsskrift* 56: 152–160.

Kaufmann, V. & R. Ladstädter (2002): Monitoring of active rock glaciers by means of digital photogrammetry. In: *Proceedings of the ISPRS Commission III Symposium "Photogrammetric Computer Vision"*, Graz, Austria, 9-13 September 2002. IAPRS 34, 3B: 108–111.

Kaufmann, V. & Ladstädter, R., 2003. Quantitative analysis of rock glacier creep by means of digital photogrammetry using multi-temporal aerial photographs: two case studies in the Austrian Alps. In: Phillips M., S.M. Springman & L.U. Arenson (eds.): *Permafrost: Proceedings of the 8th International Conference on Permafrost*, Zurich, Switzerland, 21-25 July 2003: 525–530.

Knödel, K., H. Krummel & G. Lange 1997: *Handbuch zur Erkundung des Untergrundes von Deponien und Altlasten. Band 3. Geophysik.* Bundesanstalt für Geowissenschaften und Rohstoffe. Berlin.

Krainer, K. & W. Mostler 2000: Reichenkar Rock Glacier: a Glacier-Derived Debris-Ice System in the Western Stubai Alps, Austria. P*ermafrost and Periglacial Processes* 11: 267–275.

Krainer, K. & W. Mostler 2002: Hydrology of active rock glaciers in the Austrian Alps. *Arctic, Antarctic and Alpine Research* 34: 142–149.

Krainer, K. & W. Mostler 2006: Flow velocities of active rock glaciers in the Austrian Alps. *Geografiska Annaler* 88 (a): 267–280.

Krainer, K., W. Mostler & N. Span 2002: A glacier-derived, ice-cored rock glacier in the western Stubai Alps (Austria): Evidence from ice exposures and ground penetrating radar investigation. *Zeitschrift für Gletscherkunde und Glazialgeologie* 38: 21–34.

Kraus, K. 2004: *Photogrammetrie, Band 1. Geometrische Informationen aus Photographien und Laserscanneraufnahmen.* Berlin.

Lambiel, C. & R. Delaloye 2004: Contribution of real-time kinematic GPS in the study of creeping mountain permafrost: examples from the Western Swiss Alps. *Permafrost and Periglacial Processes* 15: 229–241.

Maurer, H. & C. Hauck 2007: Instruments and Methods – Geophysical imaging of alpine rock glaciers. *Journal of Glaciology* 53, 180: 110–120.

Pillewizer, W., 1957. Untersuchungen an Blockströmen der Ötztaler Alpen. In: Fels E., H. Overbeck & J.-H. Schultze (eds.): *Geomorphologische Abhandlungen: Otto Maull zum 70. Geburtstage gewidmet.* Abhandlungen des Geographischen Institutes der Freie Universität Berlin 5. Berlin: 37–50.

Rignot, E., B. Haller & A. Fountain 2002: Rock glacier surface motion in Beacon Valley, Antarctica, from synthetic-aperture radar interferometry. *Geophysical research letters* 29, 12: 48-1–48-4. doi:10.1029/2001GL013494.

Roer, I. 2005: *Rock glacier kinematics in a high mountain geosystem.* Dissertation. Department of Geography, University of Bonn.

Roer, I., W. Haeberli, M. Avian, M. Kaufmann, R. Delaloye, C. Lambiel & A. Kääb 2008: Observations and considerations on destabilizing active rock glaciers in the European Alps. In: Kane, D.L. & K.M. Hinkel (eds.): *Proceedings of the Ninth International Conference on Permafrost*, Fairbanks, Alaska, 29 June-3 July 2008. Vol. 2: 1505–1510.

Scambos, T.A., G. Kvaran & M.A. Fahnestock 1999: Improving AVHRR resolution trough data cumulation for mapping polar ice sheets. *Remote sensing of environment* 69: 56–66.

Scambos, T.A., M.J. Dutkiewitcz, J.C. Wilson & R.A. Bindschadler 1992: Application of image cross-correlation software to the measurement of glacier velocity using satellite data. *Remote sensing of environment* 42: 177–186.

Schneider, B. & H. Schneider 2001: Zur 60jährigen Messreihe der kurzfristigen Geschwindigkeitsschwankungen am Blockgletscher im Äußeren Hochebenkar. *Zeitschrift für Gletscherkunde und Glazialgeologie* 37, 1: 1–33.

Stearns, L. & G. Hamiltom 2005: A new velocity map for Byrd Glacier, East Antarctica, from sequential ASTER satellite imagery. *Annals of glaciology* 41: 71–76.

Strozzi, T., A. Kääb & R. Frauenfelder 2004: Detecting and quantifying mountain permafrost creep from in-situ, airborne and spaceborn remote sensing methods. *International journal of remote sensing* 25, 15: 2919–2931.

Vietoris, L. 1958: Der Blockgletscher des Äußeren Hochebenkares. *Gurgler Berichte* 1: 41–45.

Vietoris, L. 1972: Über die Blockgletscher des Äußeren Hochebenkars. *Zeitschrift für Gletscherkunde und Glazialgologie* 8: 169–188.

Vitek, J.D. & J.R. Giardino 1987: Rock glaciers: a review of the knowledge base. In: Giardino, J.R., J.F. Shroder Jr. & J.D. Vitek (eds.): *Rock Glaciers.* London: 1–6.

Wehr, A. & U. Lohr 1999: Airborne laser scanning – an introduction and overview. *ISPRS Journal of photogrammetry and remote sensing* 54: 68–82.

Whalley, W.B. & H.E. Martin 1992: Rock glaciers: II models and mechanics. *Progress in physical geography* 16: 127–186.